

Patellofemoral joint contact forces  
during weight-bearing activities: a  
direct comparison of different  
biomechanical estimation methods



Thesis manuscript

# Patellofemoral joint contact forces during weight-bearing activities: a direct comparison of different biomechanical estimation methods

by

Chantal Eenkhoorn

4716868

Master Thesis Biomedical Engineering (BM51032)

Department of Biomechanical Engineering  
Faculty of Mechanical, Maritime and Material Engineering  
Delft University of Technology  
BioMechaMotionlab

To be defended on October 15<sup>th</sup>, 2019

Thesis Committee:

Prof. dr. ir. J. Harlaar

TU Delft, supervisor

Dr. E.M. Macri

Erasmus MC, co-supervisor

Prof. dr. ir. H.H. Weinans

TU Delft

Dr. ir. A. Seth

TU Delft



## Abstract

**BACKGROUND:** Knee problems are the most common complaints of the lower extremity in the Netherlands. Osteoarthritis has the highest prevalence of all knee complaints. Knee osteoarthritis is likely to start at the patellofemoral joint and is associated with the aggravation of pain. Mechanical overloading is hypothesized to contribute to the development and progression of patellofemoral osteoarthritis (PFOA). Several studies have explored the mechanical loading pattern of the patellofemoral joint. Because different biomechanical models were used, vastly different estimations of the patellofemoral joint contact force (PFJCF) were concluded. This diversity prevents a clear understanding of the role of mechanical overloading in PFOA, since it is unknown how different biomechanical models affect the PFJCF estimation.

**OBJECTIVES:** This study will explore how different biomechanical models of the patellofemoral joint affect the estimated PFJCF for common weight-bearing activities.

**METHODS:** Ten healthy participants were included in this study. Common weight-bearing activities (walking, stair ascending, stair descending, sit-to-stand and stand-to-sit) were performed in the motion lab. Marker trajectory data and force plate data were collected. The data were input to biomechanical models used to estimate the quadriceps muscle force and subsequently the PFJCF. The quadriceps muscle force was estimated using the inverse dynamics and static optimization method. From there on, the PFJCF was estimated using three PFJCF to quadriceps muscle force ratios (P2QFRs), each based on a different patellofemoral joint model (i.e. van Eijden's model, Yamaguchi's model and Gill's model). For each weight-bearing activity, the peak PFJCF was obtained and the magnitude of the difference among the biomechanical models was explored.

**RESULTS:** The static optimization method resulted in a significantly higher peak PFJCF compared to the inverse dynamics method in walking (largest effect size was 0.10 BW). However, for stair descending, sit-to-stand and stand-to-sit, the inverse dynamics method resulted in a significantly higher peak PFJCF compared to the static optimization method (largest effect size was 0.45 BW, 1.17 BW, 1.25 BW, respectively). No significant difference was found for stair ascending. For walking, Yamaguchi's model resulted in a significantly higher peak PFJCF compared to van Eijden's model and Gill's model, and van Eijden's model resulted in a significantly higher peak PFJCF compared to Gill's model (largest effect size was 0.06 BW). For stair ascending, stair descending, sit-to-stand and stand-to-sit, Gill's model resulted in a significantly higher peak PFJCF compared to van Eijden's model and Yamaguchi's model. For stair descending the van Eijden's model resulted in a significantly higher peak PFJCF compared to Yamaguchi's model. The largest effect size was 0.15 BW, 0.32 BW, 0.72 BW and 0.72 BW, for respectively stair ascending, stair descending, sit-to-stand and stand-to-sit.

**CONCLUSION:** The choice of a biomechanical model has a critical effect on the estimation of the magnitude of the PFJCF. Its differences might reach half the clinical size effects when comparing control to symptomatic PF pain patients.

**Keywords:** Patellofemoral Joint Contact Force, Knee Osteoarthritis, Inverse Dynamics, Static Optimization, Patellofemoral Joint Contact Force to Quadriceps Muscle Force Ratio

## Content

Abstract .....	4
1. Introduction.....	7
1.1 Knee osteoarthritis .....	7
1.2 Functional anatomy of the patellofemoral joint .....	8
1.3 Biomechanics of the patellofemoral joint.....	9
1.4 Models of the patellofemoral joint .....	10
1.5 Quadriceps muscle force estimation.....	11
1.5.1 Directly from inverse dynamics .....	11
1.5.2 Static optimization.....	12
1.6 Patellofemoral joint contact force estimation .....	12
1.6.1 The accuracy of PFJCF estimates in the literature.....	14
1.7 Relevance .....	14
1.8 Research question .....	15
1.9 Hypothesis .....	15
2. Methods .....	16
2.1 Participants.....	16
2.2 Procedure .....	16
2.2.1 Anthropometrics .....	16
2.2.2 Exercise protocol .....	16
2.3 Instrumentation .....	17
2.3.1 Calibration .....	18
2.3.2 Marker set .....	18
2.4 Data analysis.....	19
2.4.1 Pre-processing in QTM .....	19
2.4.2 Pre-processing in MATLAB .....	19
2.4.3 Scaling in OpenSim .....	20
2.4.4 Inverse kinematics in OpenSim .....	20
2.4.5 Inverse dynamics in OpenSim .....	21
2.4.6 Static optimization in OpenSim .....	21
2.4.7 Post-processing in MATLAB.....	22
2.4.8 Descriptive analysis .....	24
2.4.9 Statistical analysis.....	24
3. Results .....	25

3.1	Participant description .....	25
3.2	Exploring the PFJCF estimation .....	25
3.3	Walking.....	27
3.4	Stair ascending .....	27
3.5	Stair descending .....	27
3.6	Sit-to-Stand.....	28
3.7	Stand-to-Sit.....	28
4.	Discussion .....	31
4.1	Clinical relevance.....	31
4.2	Interpretation of quadriceps muscle force estimation methods.....	33
4.3	Interpretation of the P2QFRs .....	35
4.4	Evaluation of the biomechanical models .....	36
4.5	Limitations.....	38
4.6	Recommendations.....	39
5.	Conclusion .....	39
	References.....	41
	Appendices .....	44
Appendix 1	Patellofemoral Joint Models .....	45
Appendix 2	Participant Characteristics.....	48
Appendix 3	Informed Consent Form .....	49
Appendix 4	Marker List.....	54
Appendix 5	List of Virtual Created Markers .....	55
Appendix 6	Individual Scaling Factors .....	56
Appendix 7	Marker weights.....	60
Appendix 8	P2QFR .....	61
Appendix 9	Plots of the estimated PFJCF .....	63
Appendix 10	Descriptive results of the peak PFJCF .....	72
Appendix 11	Abbreviations.....	73
Appendix 12	List of Figures, Tables and Equations.....	74
	Figures .....	74
	Tables.....	76
	Equations.....	77

## 1. Introduction

Knee problems are the most common complaints of the lower extremity in the Netherlands. In 2018, about 35 per 1000 persons who visited a general practitioner did this for knee complaints<sup>[1]</sup>. This included both traumatic (e.g. distortion, ligament rupture and meniscus fracture) and non-traumatic knee complaints (e.g. osteoarthritis, patellofemoral pain (PFP) and Osgood-Schlatter). Knee osteoarthritis has the highest prevalence of all knee complaints; about 40 per 1000 patient years in 2018. The incidence and prevalence of knee osteoarthritis increases strongly after middle age and the prevalence is higher in woman than in men (about 51 vs. 29 per 1000 patient years in 2018)<sup>[1]</sup>.

### 1.1 Knee osteoarthritis

Knee osteoarthritis is a degenerative disease that involves the loss of articular cartilage and remodelling of subchondral bone<sup>[2]</sup>. Common symptoms of knee osteoarthritis are knee pain, stiffness in the knee, lower limb muscle weakness and knee instability<sup>[3-5]</sup>. These symptoms can have impact on the functional ability of people, which could limit them during daily activities<sup>[3-5]</sup>. The knee joint consists of three compartments; namely the medial and lateral compartments at the tibiofemoral joint and the patellofemoral compartment (Figure 1). Knee osteoarthritis can affect all three compartments. However, it seems that the development of tibiofemoral osteoarthritis (TFOA) is preceded by isolated patellofemoral osteoarthritis (PFOA)<sup>[6, 7]</sup>. Also, radiographic and magnetic resonance imaging (MRI) studies have shown that the patellofemoral compartment of the knee contributes to the aggravation of knee osteoarthritis symptoms<sup>[8]</sup>.



**Figure 1. Osteology of the knee.** The patellofemoral joint is located at the point where the posterior surface of the patella articulates with the trochlear groove of the femur. The tibiofemoral joint is located at the point where the lateral and medial femoral condyles articulate with the tibia. Adapted from HealthPages, *Structures of the knee*<sup>[9]</sup>.

These studies outline the potentially prominent role of the patellofemoral joint in knee osteoarthritis. Knowledge of the patellofemoral joint can contribute to a better understanding of its role in the development and progression of knee osteoarthritis.

Research has outlined that the aetiology of PFOA is multifactorial, with a complex interplay among anatomical, biomechanical, psychological, social and behavioural factors<sup>[10, 11]</sup>. A common proposed theory is that mechanical overloading contributes to the development and progression of PFOA. Mechanical overloading influences the homeostasis of the articular cartilage. It causes damage to the collagen network and this leads to the loss of articular cartilage, due to a lack of the regenerative capacity<sup>[12]</sup>. Several study outcomes support the theory that mechanical overloading contributes to the aetiology of knee osteoarthritis; for example there is a relationship found between repetitive impact loading and early onset of knee osteoarthritis in young athletics<sup>[13]</sup>. Also, excessive weight in obesity, resulting in overloading, is found to be an established risk factor<sup>[14]</sup>.

## 1.2 Functional anatomy of the patellofemoral joint

The patellofemoral joint is at the point where the posterior surface of the patella articulates with the trochlear groove of the femur (Figure 1). The patella is embedded within the extensor mechanism of the knee, including its proximal quadriceps tendon and distal patellar tendon (Figure 2).

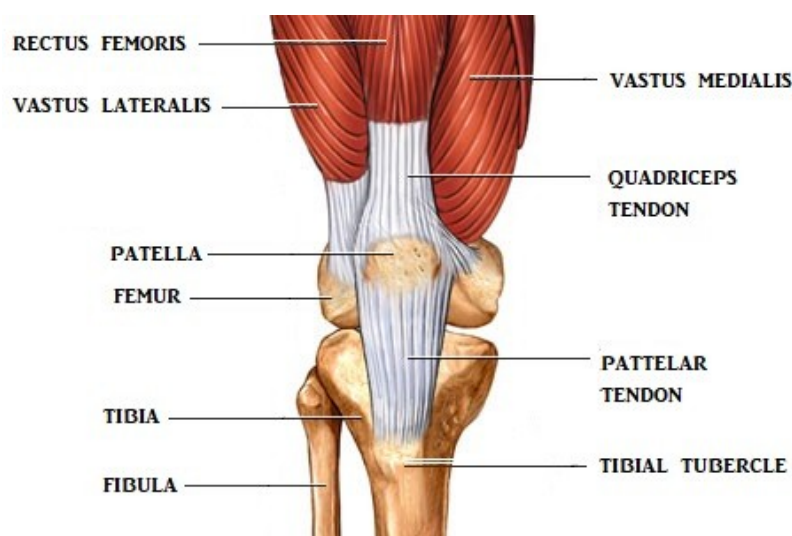


**Figure 2. The extensor mechanism of the knee.** The extensor mechanism of the knee consist of the quadriceps tendon and patellar tendon. The quadriceps tendon is formed by the quadriceps muscle group: the rectus femoris, vastus lateralis, vastus medialis and vastus intermedius (laying underneath the rectus femoris). *Adapted from Lagerman, A review of knee anatomy<sup>[15]</sup>.*

Simultaneous contraction of the quadriceps muscle group and relaxation of the flexor muscles of the knee (hamstring and gastrocnemius) causes a net extensor moment in the knee. This can lead to knee extension (e.g. when standing up from a seated position), or vice versa to knee flexion (e.g. when sitting down). The patella serves as a mechanical pulley for the quadriceps muscle, and throughout the range of motion (ROM) of the knee, the patella increases the internal moment arm of the knee extensors (i.e. in the sagittal plane) and it changes the direction of the extension force on the tibia<sup>[16]</sup>.

### 1.3 Biomechanics of the patellofemoral joint

As mentioned earlier, it is hypothesized that mechanical overloading contributes to the development and progression of PFOA. Mechanical overloading in the patellofemoral joint arises from elevated stress. The average patellofemoral joint stress (PFJS) is defined as the joint contact force per unit contact area. Elevated stress could either be the result of a decrease in the patellofemoral contact area (PFCA) and/or an increase in patellofemoral joint contact force (PFJCF). The PFCA is defined as the contact area between the two articulating surfaces of the patellofemoral joint (Figure 3). Throughout the range of motion the PFCA changes; with increased knee flexion, the point contact on the patella shifts proximally and on the trochlear groove distally. The PFCA increases from 30 to 90 degrees of knee flexion<sup>[17]</sup> and under weight-bearing conditions (e.g. caused by cartilage deformation and changes in patellar alignment)<sup>[18]</sup>.

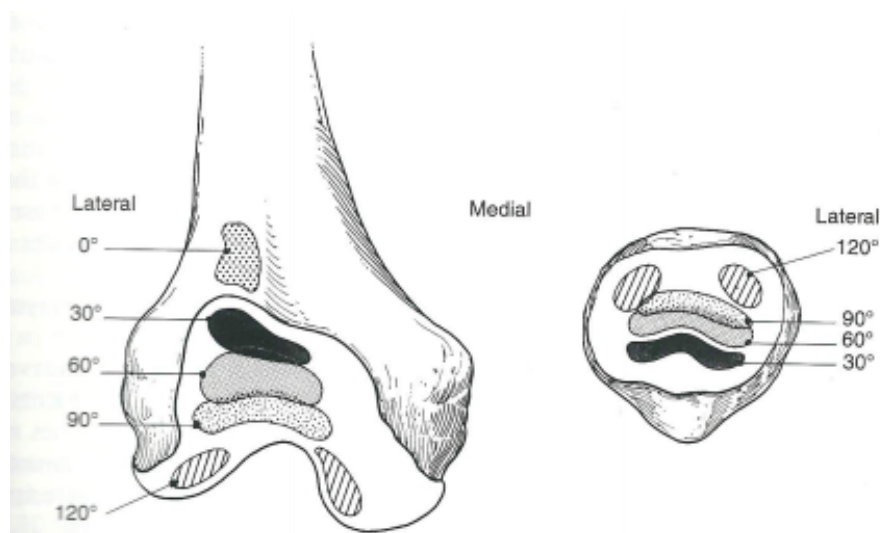
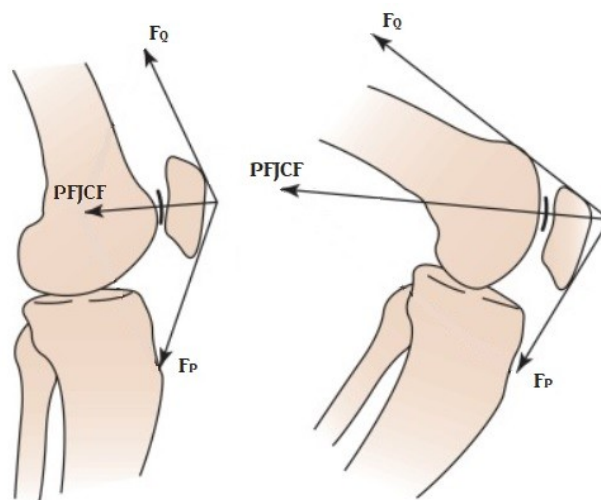


Figure 3. Patellofemoral contact area (PFCA) as a function of the knee flexion angle. Reproduced from Scuderi (1995)<sup>[17]</sup>.

The PFJCF is the compression force acting on the joint. In quasi-static situations, the PFJCF is defined as the resultant vector of both the quadriceps muscle force vector and patellar tendon force vector (Figure 4). The magnitude of the PFJCF depends on the interplay among several factors, including the knee flexion angle, knee extensor moment, knee extensor moment arm, patellar tendon force and quadriceps muscle force<sup>[19]</sup>. Also other features such as hamstrings activity, calf muscles activity, tendons, swelling, cartilage damage, patellar alignment and gravity can influence the mechanics of the patellofemoral joint<sup>[20]</sup>.

Analysing the mechanical loading pattern of the patellofemoral joint could advance our understanding of knee osteoarthritis and this could ideally be used for the management of knee osteoarthritis. A logical first step in analysing the mechanical loading would be to explore the PFJCF. The next step in analysing the mechanical loading would be to include the PFCA and explore the PFJS. The accuracy of the PFJCF estimate is crucial for the accuracy of the PFJS. Therefore, this study will focus on the first step, exploring the PFJCF.



**Figure 4. Patellofemoral joint contact force (PFJCF) in the sagittal plane as a function of the knee flexion angle and quadriceps muscle force.** PFJCF is the resultant vector of the quadriceps muscle force vector ( $F_q$ ) and the patellar tendon force vector ( $F_p$ ). Adapted from Powers, Souza & Fulkerson (2016)<sup>[21]</sup>

#### 1.4 Models of the patellofemoral joint

In earlier studies, in vitro cadaveric models have been used to experimentally estimate the PFJCF. These models provided insight into the mechanics of the patellofemoral joint<sup>[22, 23]</sup>. However, it is difficult to reproduce the loading patterns of the knee during daily activity with cadaveric models. Thus it is questionable whether the measured PFJCF under in vitro conditions can be generalized to in vivo conditions. In later studies, biomechanical models of

the patellofemoral joint have been used to estimate PFJCF. Both two-dimensional and three-dimensional models have been developed<sup>[16, 24]</sup>. In these biomechanical models, the magnitude of the PFJCF is dependent on the quadriceps muscle force and knee flexion angle.

Previous studies that used biomechanical models of the patellofemoral joint to investigate the mechanical loading had the same approach to estimate the PFJCF (and PFJS) (Figure 5). Depending on the chosen models to estimate the quadriceps muscle force and PFJCF, kinematic data (joint movements), kinetic data (ground reaction forces), electromyographic (EMG) data (of selected lower extremity muscles) or imaging data (of selected lower extremity muscles, tendons, and bones) were collected. Next, the quadriceps muscle force was estimated using a chosen method. Last, the PFJCF was estimated by using a chosen model.

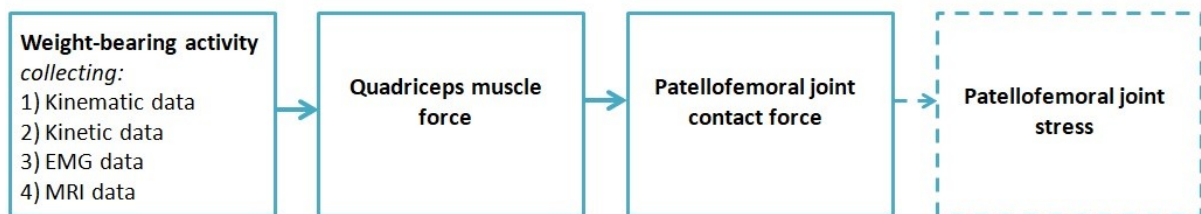


Figure 5. General approach used in studies to estimate the quadriceps muscle force and subsequently the PFJCF (and PFJS).

## 1.5 Quadriceps muscle force estimation

### 1.5.1 Directly from inverse dynamics

The simplest quadriceps muscle force estimation method uses the knee extensor moment. First, the knee extensor moment is derived from an inverse dynamics approach (e.g. Newton-Euler approach). In this approach the movement is known and the forces and moments that create these movements are the unknowns that need to be calculated. These unknowns can be calculated by applying equations of motions<sup>[25]</sup>. Second, the knee extensor moment is divided by the moment arm of the quadriceps muscle in order to estimate the quadriceps muscle force (Equation 1).

$$1 \quad F_{quad} = \frac{KEM}{EQma}$$

$F_{quad}$  = quadriceps muscle force,  $KEM$  = knee extensor moment,  $EQma$  = effective moment arm of the quadriceps muscle

To include both the leverage and spacing function of the patella, the effective moment arm of the quadriceps muscle has been used extensively<sup>[16, 26, 27]</sup>. The effective moment arm is defined as the product of the actual moment arm (perpendicular distance from the patellar tendon to the tibiofemoral contact point) and the ratio of the patellar tendon force to quadriceps muscle force (Equation 2). A drawback of estimating the quadriceps muscle force from the knee extensor moment is that it does not take into account muscle co-contractions. Therefore, the quadriceps muscle force will be underestimated.

$$2 \quad EQma = AQma \times \frac{F_{pt}}{F_{quad}}$$

EQma= effective moment arm of the quadriceps muscle. AQma = actual moment arm of the quadriceps muscle, F<sub>pt</sub>/F<sub>quad</sub> = ratio of patellar tendon force to quadriceps muscle force

### 1.5.2 Static optimization

Another method to estimate the quadriceps muscle force is by means of static optimization. With static optimization individual muscle forces are estimated from the joint moments. The musculoskeletal system is a redundant system, which implies that there are more muscles present in the system than there are degrees of freedom. Therefore, optimization is necessary to solve the load-sharing problem (different combinations of muscles forces can compute the same joint moments). During static optimization, a certain cost function (e.g. sum of squared muscle forces) is minimized for each time step in order to find a unique solution of individual muscle forces that compute the moments<sup>[25]</sup>. Thus, the static optimization approach takes into account the load sharing problem and muscle co-contractions at multiple joints. Therefore, this method seems to result in a more realistic estimate of the quadriceps muscle force compared to the inverse dynamics method.

### 1.6 Patellofemoral joint contact force estimation

Previous studies estimated the PFJCF by multiplying the estimated quadriceps muscle force with the PFJCF to quadriceps muscle force ratio (P2QFR). Several biomechanical models of the patellofemoral joint have been developed that provide an expression of the P2QFR. In Textbox 1 a comparison among the biomechanical models of van Eijden, Kouwenhoven and Verburg (1986)<sup>[27]</sup>, Yamaguchi and Zajac (1989)<sup>[16]</sup> and Gill and O'Conner (1996)<sup>[26]</sup> is given.

**TEXTBOX 1**  
**Patellofemoral joint models**

Van Eijden’s model, Yamaguchi’s model and Gill’s model provide a comprehensive picture of the mechanics of the patellofemoral joint in the sagittal plane (Table T1, Appendix 1).

All three models are applicable to static situations. Yamaguchi’s model simulates the patellofemoral joint within the smallest knee flexion range, from zero until 90 degrees, followed by van Eijden’s model, from zero until 120 degrees. Gill’s models simulates the patellofemoral joint within the biggest knee flexion range, from zero until 140 degrees. Van Eijden’s model and Gill’s model both include tendofemoral contact at high knee flexion angles. In van Eijden’s model this occurs at 80 degrees of knee flexion and in Gill’s model at 87.5 degrees of knee flexion. Yamaguchi’s model does not include tendofemoral contact. All three models consider the patella, femur and tibia as rigid bodies. In van Eijden’s and Gill’s model the femur is assumed to be fixed, while in Yamaguchi’s model the tibia is assumed to be fixed. The patellar tendon has a constant length in all three models. Also it is assumed that a single point of contact occurs between the articular surfaces. In Gill’s model the patella has two articular surfaces. The first articular surface is formed by the central median ridge of the patella with the trochlear groove, the second articular surface is formed between the medial and lateral facets of the patella and medial and lateral femoral condyles (at high knee flexions). While the tibiofemoral contact point is used as reference point about which the moment calculations are made in van Eijden’s and Yamaguchi’s model, the intersection point of the line of action of the anterior and posterior cruciate ligaments is used as reference point in Gill’s model. The system parameters of van Eijden’s model were based on ten males, of Gill’s model on four healthy adults and of Yamaguchi’s model on one scaled male. With all three models the P2QFR, patellar tendon to quadriceps force ratio (PT2QFR), the patellar axis and patellar tendon orientation can be estimated. With van Eijden’s model and Yamaguchi’s model also the quadriceps tendon orientation can be estimated. With van Eijden’s model and Gill’s model also the location of the patellofemoral contact point can be estimated. With Yamaguchi’s model and Gill’s model the actual moment arm of the patellar tendon and effective moment arm of the quadriceps tendon can be estimated. And with Gill’s model the patellar mechanism angle, the angle between the lines of action of the patellar tendon force and quadriceps tendon force, can also be described.

**Table T 1. Features of the patellofemoral joint models.**

Key features	Van Eijden	Yamaguchi	Gill
<b>State</b>	static	static	static
<b>Range of motion</b>	from zero until 120 degrees of knee flexion	from zero until 90 degrees of knee flexion	from zero until 140 degrees of knee flexion
<b>Tendofemoral contact</b>	Yes	No	Yes
<b>Rigid bodies</b>	patella (free) femur (fixed) tibia (free)	patella (free) femur (free) tibia (fixed)	patella (free) femur (fixed) tibia (free)
<b>Patellar tendon</b>	fixed length	fixed length	fixed length
<b>Contact points</b>	single point	single point	single point
<b>Reference point moment calculations</b>	Tibiofemoral contact point	Tibiofemoral contact point	Intersection point of the line of actions of the anterior and posterior cruciate ligaments
<b>System parameters</b>	10 male knees	1 scaled male knee	4 healthy adults knees
<b># equations</b>	nine non linear	three non linear	not specified
<b>Output</b>	1. P2QFR 2. PT2QFR 3. patellar axis orientation 4. patellar tendon orientation 5. quadriceps tendon orientation 6. patellofemoral contact point location	1. P2QFR 2. PT2QFR 3. patellar axis orientation 4. patellar tendon orientation 5. quadriceps tendon orientation 6. Actual moment arm of the patellar tendon 7. Effective moment arm of the quadriceps muscle	1. P2QFR 2. PT2QFR 3. patellar axis orientation 4. patellar tendon orientation 5. patellar mechanism angle 6. patellofemoral contact point location 7. Actual moment arm of the patellar tendon 8. Effective moment arm of the quadriceps muscle

The differences in modelling approach have influence on the P2QFR provided by the studies. For all studies the P2QFR has a minimum value at maximal extension. The minimum value was for van Eijden's model, Yamaguchi's model and Gill's model, 0.50, 0.49 and 0.37, respectively. The continuation of the P2QFR slope differs for the three models. The P2QFR of Yamaguchi's model increases until 60 degrees of knee flexion to 0.96 and from 60 until 90 degrees of knee flexion it stays more or less equal. The P2QFR of van Eijden's model increases until 80 degrees of knee flexion to 1.00 and from 80 until 120 degrees of knee flexion it stays more or less equal. The P2QFR of Gill's model increases until 110 degrees of knee flexion to 1.17 and from 110 until 140 degrees of knee flexion it decreases to 1.13. The difference in P2QFR will have their influence on the estimated PFJCF.

#### **1.6.1 The accuracy of PFJCF estimates in the literature**

In the literature there are several studies that have estimated the PFJCF during weight-bearing activities. This has been done in healthy control groups as well as in patellofemoral disease groups. The concluded PFJCF values, for the same population group and activity, vary among studies. Reilly and Martens (1972)<sup>[28]</sup> reported a peak PFJCF equal to 7 times bodyweight (BW) for squatting. However, Escamilla, Fleisig and Zheng (2001)<sup>[29]</sup> reported a mean peak PFJCF of 2.1 times BW for squatting. For jumping, Simpson, Jameson and Odum (1996)<sup>[30]</sup> reported a PFJCF of 10.4 times BW, while Cleather, Goodwin and Bull (2013)<sup>[31]</sup> reported a PFJCF of 4.2 times BW. The vastly different results concluded across these studies call into question the validity of the methods used in at least some of the studies, and prevent a clear understanding of the role that PFJCF may play in the aetiology of patellofemoral disease.

### **1.7 Relevance**

Without knowledge of the underlying models that are used in the studies to estimate the PFJCF, the results of the studies may be misinterpreted and incorrectly used in for example rehabilitation programs. Therefore, it would be informative to explore the magnitude of the difference in PFJCF estimation due to the use of different biomechanical models. This information can be relevant when determining whether the use of different biomechanical models to estimate the PFJCF will lead to a meaningful difference (statistically or clinically). Also, this information can be used to determine whether different estimation methods can be used interchangeably or if a particular estimation method is more appropriate.

## 1.8 Research question

The research question is formulated as follow:

*What is the effect of using different biomechanical models on the estimation of the PFJCF in common weight-bearing activities?*

To answer this research question the following sub-questions will be answered for each weight-bearing activity:

1. *What is the effect of using different methods to estimate quadriceps muscle force?*
2. *What is the effect of using different P2QFR models?*

## 1.9 Hypothesis

The following hypotheses were formulated for the sub-questions:

1. It is hypothesized that the static optimization method will result in higher quadriceps muscle force estimations and subsequently in higher PFJCF estimations compared to the inverse dynamics methods.
2. It is hypothesized that Gill's model will result in higher PFJCF estimations above 60 degrees of knee flexion and in lower PFJCF estimations below 60 degrees of knee flexion compared to van Eijden's model and Yamaguchi's model. Furthermore, it is hypothesized that van Eijden's model will results in higher PFJCF estimations above 60 degrees of knee flexion and in lower PFJCF estimations below 60 degrees of knee flexion compared to Yamaguchi's model.

## **2. Methods**

### **2.1 Participants**

In this study, ten healthy adults were included (six women and four men). The participants had a mean age of 27.1 (SD 7.4) years, a mean length of 176.6 (SD 10.6) cm and a mean weight of 70.1 (SD 11.1) kg. The characteristics of each participant can be found in Appendix 2. Before the start of the experiment the participants were informed about the procedure and they provided informed written consent (Appendix 3). The experimental protocol was approved by the Human Research Ethics Committee of the Delft University of Technology (TU Delft).

### **2.2 Procedure**

#### **2.2.1 Anthropometrics**

The height (Frankfurt plane position) (Seca, 206) and the weight (Omron, HN-289) of the participant were measured.

#### **2.2.2 Exercise protocol**

Participants were asked to perform five different weight-bearing dynamic activities, namely walking, stair ascending, stair descending, sit-to-stand and stand-to-sit. For each activity five correct trials were conducted for both the left and right leg, resulting in ten correct trials per participant for each activity. A trial was remarked as correct when proper marker trajectory data and force plate data were collected.

During the walking task, participants walked at a self-selected speed along a 8.4m runway that included two, in series placed, force plates (60x50 cm) (Figure 6A). Participants were instructed to walk at their normal walking speed and to look straight ahead at a visual target when walking.

For the stair ascending and stair descending tasks, a two step staircase (height 21cm, tread 30 cm) was used. The staircase included one smaller force plate (30x50cm) located on the first step (Figure 6B). At the start of the stair ascending task the participants stood in front of the staircase, and at the start of the stair descending task the participant stood on the second step of the staircase. For both activities the participants were instructed to use a step-over-step strategy, meaning that one foot is placed on each stair during stair ambulation. Also, they were instructed to perform the activity at their own preferred speed.

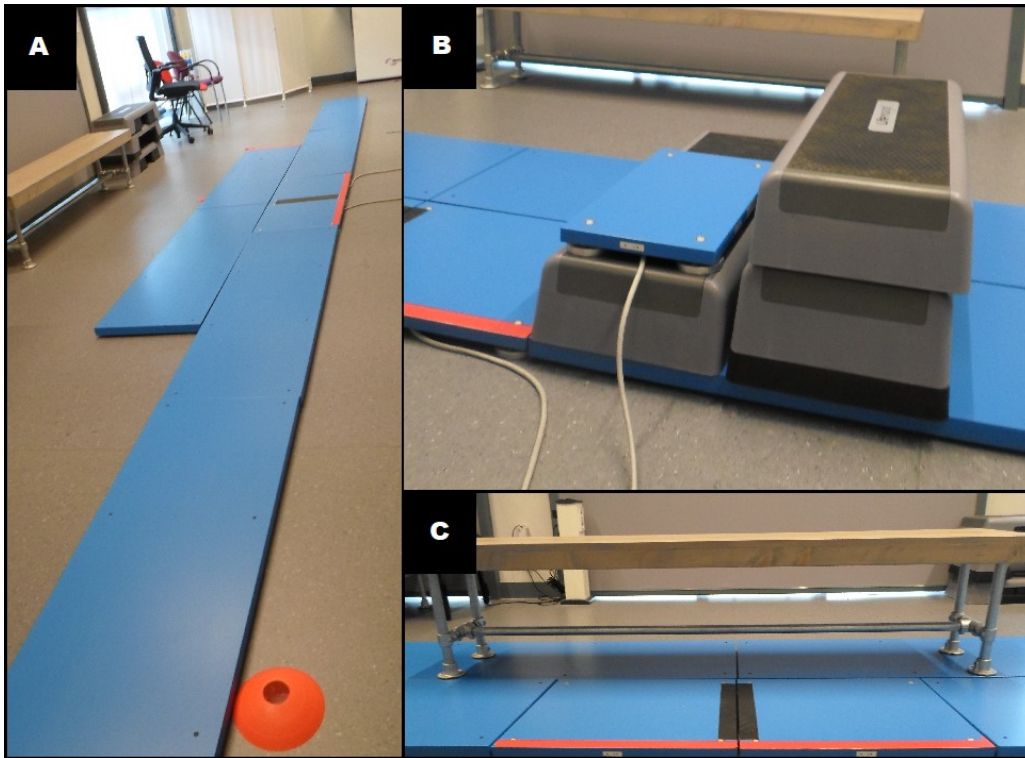


**Figure 6. Experimental set-up.** Panel A shows the 8.4m runway used in the walking task. Panel B shows the staircase used for the stair ascending and stair descending tasks. Panel C shows the bench used for the sit-to-stand and stand-to-sit task.

A bench with a height of 48cm was used for the sit-to-stand and stand-to-sit tasks. The bench was positioned adjacent to the force plates of the runway such that it did not have contact with the force plates (Figure 6C). At the beginning of each trial participants rested their feet on an aerobic step in front of the bench, to ensure that there was no force on the force plates at the start of the trial. Participants were asked to stand up from the bench and to sit down again at a self-selected speed. They were instructed to place their hands on the opposite shoulders, to keep their feet flat on the floor, and to maintain a straight back.

### 2.3 Instrumentation

The motion analysis was performed in the BioMechaMotion lab at the TU Delft. Three-dimensional lower extremity marker trajectory data were collected using a motion capture system consisting of 12 marker-tracking cameras with a sampling rate of 100Hz and two video cameras with a sampling rate of 24 Hz (Qualisys AB, Göteborg, Sweden). Ground reaction force data were collected at a sampling rate of 1000 Hz using force plates (9260AA, Kistler, Winterhur, Switzerland). Marker trajectory data and ground reaction force data were acquired using an integrated synchronized data stream in real-time controlled by motion capture software (Qualisys Track Manager Version 2019.1, Qualisys AB).

### 2.3.1 Calibration

Prior to the experiments, the motion capture system was calibrated. An L-shaped reference bar was placed on one of the force plates to determine the origin on the ground. The x-axis pointed in the walking direction, the y-axis pointed to the left and the z-axis pointed upwards. A T-shaped calibration wand (600 mm) was then used to calibrate the measurement volume (in all three dimensions) for 120 seconds.

### 2.3.2 Marker set

39 passive spherical markers (9.5 mm diameter) were placed according to the lower extremity marker set shown in Figure 7 and Appendix 4. The lower extremity was divided into seven segments and 6 joints. The marker set consisted of anatomical markers and tracking markers. The anatomical markers were placed on anatomical landmarks of the body. At each segment there were at least three anatomical markers. This was necessary to track the six degree of freedom motion of each body segment.

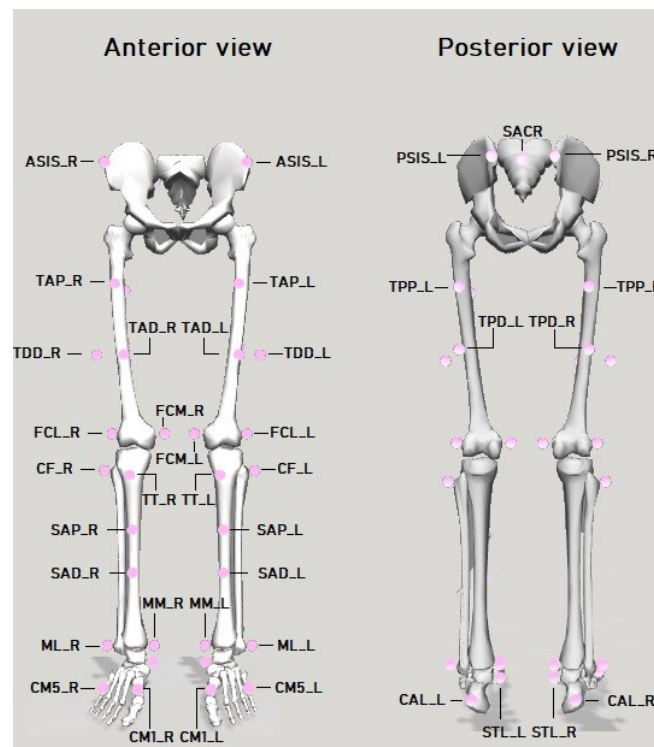


Figure 7. Marker set of the lower extremity.

First, a static calibration trial was performed to define the segments and joint axes. After the static trial, the markers needed solely for anatomical calibration were removed (medial malleoli and medial femoral epicondyles). Subsequently, a dynamic calibration trial was

performed. The dynamic calibration trial was used to train automatic identification of markers (the AIM model) in Qualisys Track Manager software (QTM).

## 2.4 Data analysis

### 2.4.1 Pre-processing in QTM

Marker trajectory data were pre-processed using QTM. Firstly, the marker trajectories were labelled. An AIM model was created and this model was applied to all the trials in order to identify the markers. If necessary, the labelling was adjusted by hand. Secondly, gaps in the marker trajectory data were filled using spline interpolation. Thirdly, events were identified in order to normalize the data to a cycle. For the walking, stair ascending and stair descending trials, the initial contact and toe off events on the force plate were identified, such that the cycle was normalized to the stance phase of respectively walking, stair ascending and stair descending. For the sit-to-stand and stand-to-sit, the trial was normalized from initiating standing till full standing and from initiating sitting till full sitting. After the pre-processing steps were finished, the data were exported as a MATLAB data file containing marker trajectory data, force plate data and events.

### 2.4.2 Pre-processing in MATLAB

MATLAB software (MATLAB r2018b, The MathWorks, Inc., Natick USA) was used to write scripts to prepare the marker trajectory and force plate data for OpenSim software. Marker trajectory data were low pass filtered at 6Hz using a fourth-order Butterworth filter. Force plate data were low pass filtered at 8Hz using a fourth-order Butterworth filter. Virtual markers were created (see 2.4.3 Scaling in OpenSim). The data were transformed from the coordinate system of the motion capture system into the coordinate system of the OpenSim software (Figure 8). Marker trajectory data were written into .sto files and the force plate data were written into .mot files, both input format files for OpenSim.



**Figure 8. The coordinate systems used in QTM and OpenSim.** The output data of QTM had to be rotated towards the OpenSim coordinate system; with the y-axis pointing upwards, the x-axis pointing forwards, the z-axis pointing to the right.

### 2.4.3 Scaling in OpenSim

The OpenSim Scale tool (OpenSim 4.0) was used to create participant-specific models for each participant out of the generic 2392 gait model of OpenSim. The generic 2392 gait model is a three-dimensional computer model of the human musculoskeletal system. The model has 23 degrees-of-freedom and 92 musculotendon actuators that represent 76 muscles in the lower extremities and torso<sup>[32]</sup>.

First, a model marker set was created for the generic 2392 gait model. This model marker set consisted of the 39 experimental markers (anatomical and tracking markers) and of 20 virtual markers that were calculated from the experimental collected markers (Appendix 4 & Appendix 5). The virtual created markers were needed to scale the generic 2392 gait model into participant-specific models. Second, the distance between chosen marker pairs from the model marker set and the distance between marker pairs from the participants marker set were used to compute scale factors (Table 1). These scale factors were used to scale the dimensions of each segment. Individual participant scaling factors can be found in Appendix 6. The masses of the segments were scaled proportionally. The mass of all segments equalled the total mass of the participant. Also, muscle fiber lengths and tendon slack lengths were scaled, such that the ratio relative to the total actuator length remained the same<sup>[33]</sup>.

**Table 1 Scaling pairs used in OpenSim.** For the pelvis, talus, calcaneus and toes three scaling pairs were calculated for all directions. For the femur and tibia two scaling pairs were calculated, in the superior/inferior and medial/lateral directions. The anterior/posterior direction was scaled with the scale factor of the medial/lateral direction. *Acronyms are described in Appendix 4 and Appendix 5.*

Segment	Scaling pairs		
	<i>anterior/posterior</i>	<i>superior/inferior</i>	<i>medial/lateral</i>
<b>Pelvis</b>	PSIS_MID, ASIS_MID	HJC_MID, PELVIS_MID	HJC_R, HJC_L
<b>Femur (L/R)</b>	FCM, FCL	HJC, KJC	FCM, FCL
<b>Tibia (L/R)</b>	MM, ML	KJC, AJC	MM, ML
<b>Talus (L/R)</b>	P_CAL, P_MID-CM	P_AJC, AJC	P_CM5, P_CM1
<b>Calcaneus (L/R)</b>	P_CAL, P_MID-CM	P_AJC, AJC	P_CM5, P_CM1
<b>Toes (L/R)</b>	P_CAL, P_MID-CM	P_AJC, AJC	P_CM5, P_CM1
<b>Torso</b>	unassigned		

### 2.4.4 Inverse kinematics in OpenSim

The participant-specific model with associated model marker set was then used to solve an inverse kinematics problem. This model marker set consisted of the 35 experimental markers with a tracking purpose (Appendix 4) and of two virtual markers (right and left hip

joint center markers). The inverse kinematics algorithm describes a least-squares problem, where for each time step the marker error, the difference in distance between the experimental measured markers and virtual model markers, was minimized. Weights were given to the markers that specified how strongly the marker error was minimized (Equation 3, Appendix 7). The output data contained joint angles (generalized coordinates) over time<sup>[34]</sup>. The knee angle over time was the output of interest for this study.

$$3 \quad \min_q \left[ \sum_{i \in \text{markers}} w_i |x_i^{\text{exp}} - x_i(q)|^2 \right]$$

$q_j$  = vector of generalized coordinates,  $x_i^{\text{exp}}$  = experimental position of marker  $i$ ,  $x_i(q)$  = position of the corresponding model,  $w_i$  = weight of marker  $i$

#### 2.4.5 Inverse dynamics in OpenSim

With the inverse dynamics tool, the joint moments for each time step were determined. The generated participant-specific model, joint angles (estimated with the inverse kinematics step) and filtered experimental ground reaction force data were used to solve the equations of motion for the unknown generalized forces (Equation 4)<sup>[35]</sup>. The knee moment over time was the output of interest for this study.

$$4 \quad M(q)\ddot{q} + C(q, \dot{q}) + G(q) = \tau$$

$q$  = vector of generalized positions,  $\dot{q}$  = vector of generalized velocities,  $\ddot{q}$  = vector of generalized acceleration,  $M(q)$  = system mass matrix  $C(q, \dot{q})$  = vector of Coriolis and centrifugal forces,  $G(q)$  = vector of gravitational forces,  $\tau$  = vector of generalized forces

#### 2.4.6 Static optimization in OpenSim

The static optimization tool was used to estimate individual muscle forces over time. This was done by minimizing the sum of squared muscle activations, that was constrained by muscle force-velocity and force-length properties (Equations 5&6). The generated participant-specific model, joint angles (estimated with the inverse kinematics step) and filtered experimental ground reaction force data served as input for the static optimization tool. Also residual actuators, for each degree of freedom, were added to the ground pelvis joint. These residual actuators were required because there was a dynamic inconsistency between the model accelerations, estimated from measured marker kinematics, and the experimentally measured ground reaction force data of the participant. If the muscles were too weak, coordinate actuators were added to the joints in the model<sup>[36]</sup>. The quadriceps muscle force over time was the output of interest of this study.

$$5 \quad \sum_{m=1}^n = [a_m f(F_m^0, l_m, v_m)] r_{m,j} = \tau_j$$

n= number of muscles in the model,  $a_m$  = the activation level of muscle m at the discrete time step,  $f(F_m^0, l_m, v_m)$  = force-length-velocity surface of muscle m,  $r_{m,j}$  = moment arm of muscle m around the joint axis.  $\tau$  = the generalized force acting about the joint axis, p = user defined constant.

$$6 \quad J = \sum_{m=1}^n (a_m)^p$$

n= number of muscles in the model,  $a_m$  = the activation level of muscle m at the discrete time step, p = user defined constant

#### 2.4.7 Post-processing in MATLAB

All data were saved in a data structure. The time series of knee angle, knee extensor moment and quadriceps muscle force data from OpenSim were normalized over stride, using the gait events that were labelled in QTM. The knee angle was reversed, such that knee flexion was represented by positive angle values and knee extension was represented by negative angle values. The knee extensor moment, derived from the inverse dynamics step, and the quadriceps muscle force, derived from the static optimization step, were divided by the mass of the participant and gravity in order to get the moment and force in BW. From now on the quadriceps muscle force derived from the static optimization method will be referred to as *the static optimization method*.

#### *Estimating the quadriceps muscle force directly from inverse dynamics*

In order to estimate the quadriceps muscle force, the knee extensor moment derived from inverse dynamics was divided by the effective moment arm of the quadriceps muscle (Equation 1). The effective moment arm, as a function of knee flexion angle, was estimated using a formula proposed by Brechter and Powers (2002)<sup>[37]</sup> (Equation 7). This formula was based on the effective moment arm graph of van Eijden, Weijs and Kouwenhoven (1987)<sup>[38]</sup>. From now on the quadriceps muscle force derived from the inverse dynamics method will be referred to as *the inverse dynamics method*.

$$7 \quad EQma = 8.0e^{-5}\theta^3 - 0.013\theta^2 + 0.28\theta + 46.2$$

EQma = effective moment arm of the quadriceps muscle in mm,  $\theta$  = knee flexion angle in degrees

#### *Estimating the PFJCF*

In order to estimate the PFJCF, the quadriceps muscle force estimate was multiplied by the P2QFR. Three different functions that describe the P2QFR were used. These functions were

based on three different biomechanical models of the patellofemoral joint; the models of van Eijden et al. (1986)<sup>[27]</sup>, Yamaguchi et al. (1989)<sup>[16]</sup> and Gill et al. (1996)<sup>[26]</sup> (Figure 9).

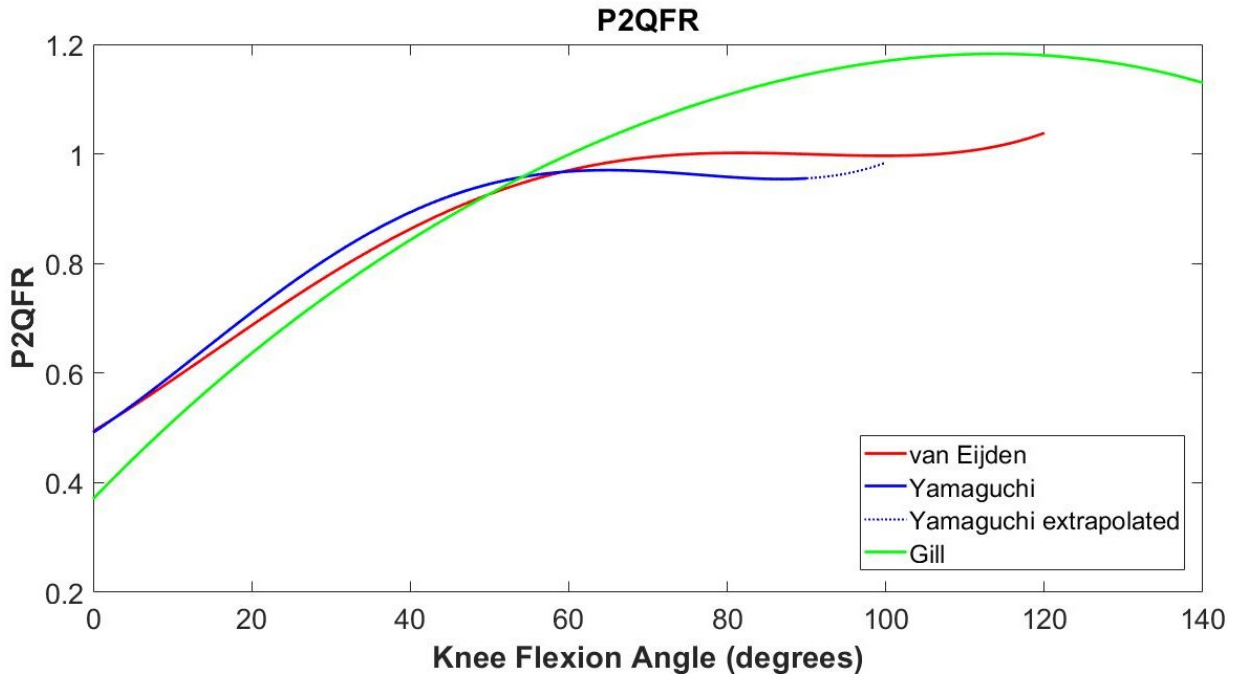


Figure 9. P2QFR for van Eijden's, Yamaguchi's and Gill's model as a function of knee flexion angle. The ratio for Yamaguchi's model is extrapolated from 91 until 100 degrees of knee flexion.

For van Eijden's model the function of the P2QFR developed by Nunes, Silva and dos Santos (2018)<sup>[39]</sup> was used (Equation 8). It describes the mean value of the P2QFR as a function of the knee flexion angle.

$$8 \quad \text{P2QFR} = 2.70e^{-2}\theta^4 + 1.96e^{-2}\theta^3 - 0.15\theta^2 + 0.13\theta + 0.97$$

P2QFR = ratio of PFJCF to quadriceps muscle force,  $\theta$  = normalization of knee flexion angle (in degrees)

For Yamaguchi's model and Gill's model we had to rely on the graphical results of the P2QFR represented in their papers. These graphical results were digitized using the MATLAB function Grabit. From that data a function was derived using the Curve Fitting Toolbox of MATLAB (Appendix 8). Equation 9 shows the P2QFR based on Yamaguchi's model and Equation 10 shows the P2QFR based on Gill's model.

$$9 \quad \text{P2QFR} = 0.21e^{-1}\theta^4 - 2.77e^{-5}\theta^3 - 0.14\theta^2 + 0.16\theta + 0.92$$

P2QFR = ratio of PFJCF to quadriceps muscle force,  $\theta$  = normalization of knee flexion angle (in degrees)

$$10 \quad P2QFR = -0.44e^{-2}\theta^4 - 4.55e^{-4}\theta^3 - 0.12\theta^2 + 0.24\theta + 1.06$$

P2QFR = ratio of PFJCF to quadriceps muscle force,  $\theta$  = normalization of knee flexion angle (in degrees)

### **Peak PFJCF**

From the PFJCF the peak PFJCF was extracted. This was done for all trials of each individual in order to estimate the average peak PFJCF (for each weight-bearing activity).

#### **2.4.8 Descriptive analysis**

The peak PFJCF, standard deviation (SD), standard error of the mean and 95% confidence interval were determined for each weight-bearing activity. The absolute and relative differences in peak PFJCF among the different estimation methods were also determined. The relative difference was described relative to the mean of the different estimation methods.

#### **2.4.9 Statistical analysis**

For each weight-bearing activity a statistical analysis was performed to determine:

1. whether the static optimization method or inverse dynamics method resulted in a significantly different peak PFJCF.
2. whether the different P2QFRs, based on van Eijden's model, Yamaguchi's model and Gill's model, resulted in a significantly different peak PFJCF.

A significance level of  $p < 0.05$  was used. A two-way repeated ANOVA was performed for each weight-bearing activity. The quadriceps muscle force estimation methods and the P2QFR models were the within-subject independent variables. Levene's test was used to check if the variance was equal. Mauchly's sphericity test was used to assess whether the sample variances of the repeated measurements were equal and if the sample correlations among all pairs of measures were equal. If sphericity was violated, adjusted results were used to account for a possible increase in Type 1 error (the rejection of a true null hypothesis). The Greenhouse-Geisser correction was then used. The data were analysed in IBM SPSS statistics (Version 25.0 Armonk, NY: IBM Corp.)

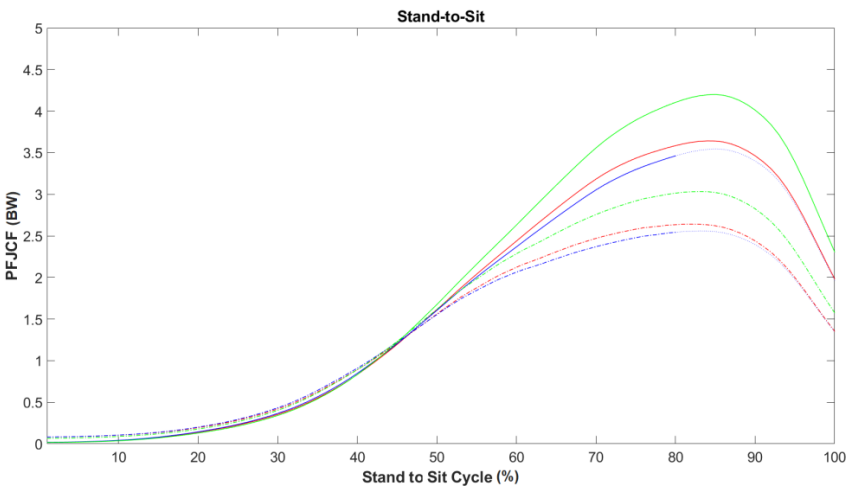
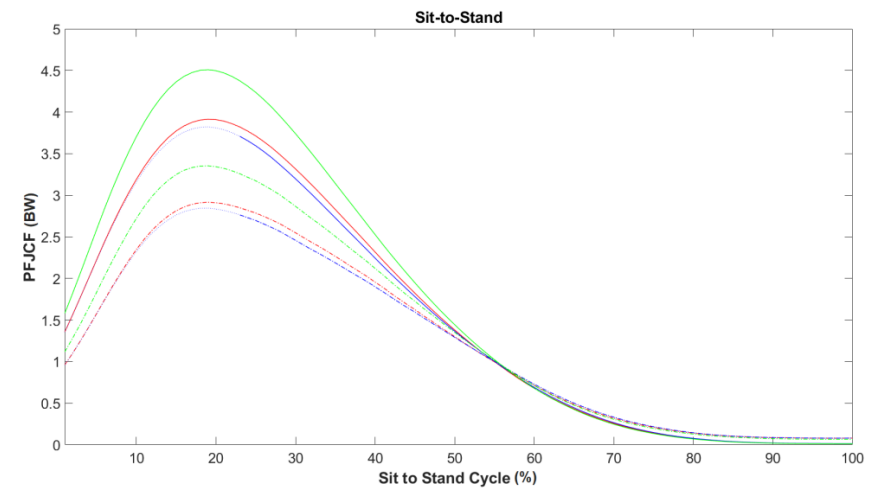
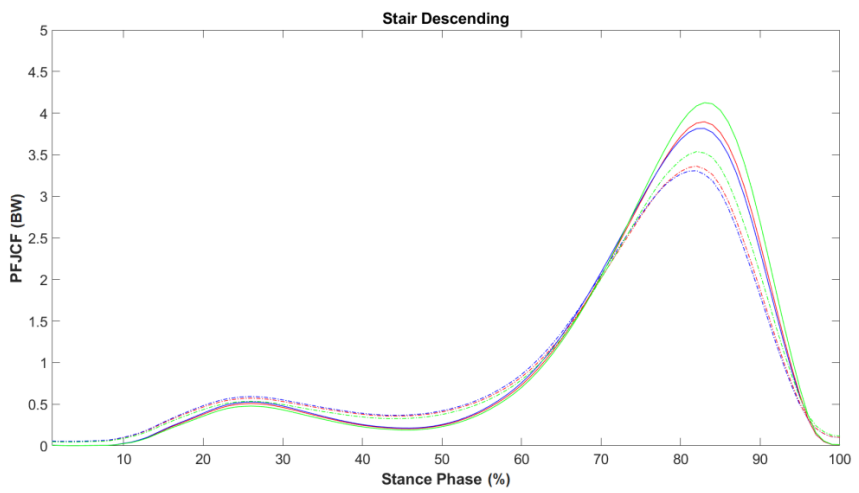
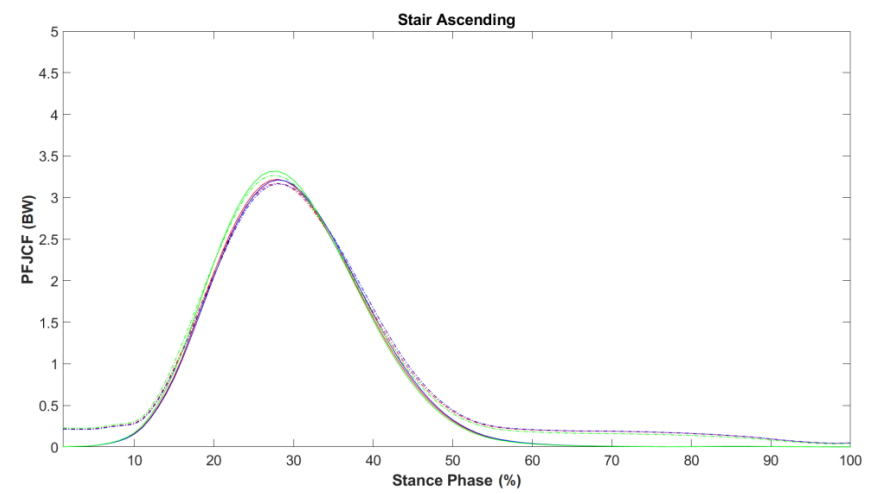
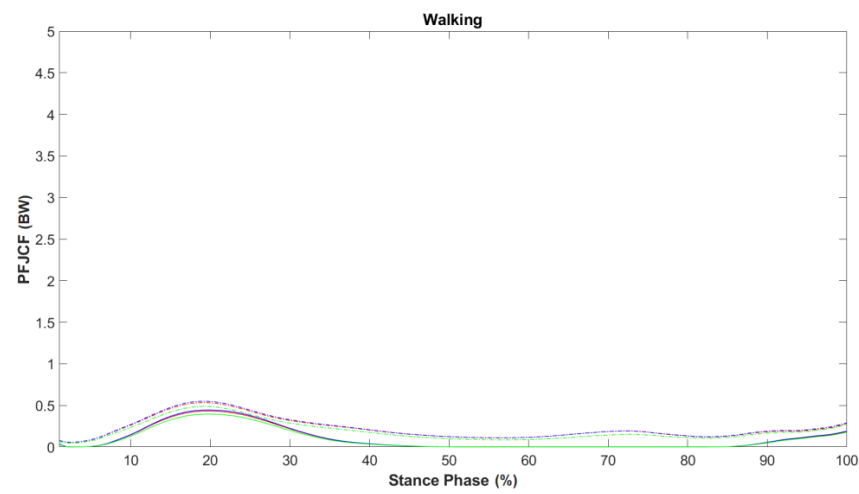
### **3. Results**

#### **3.1 Participant description**

Eleven healthy adults participated in this study. Ten out of eleven participants were included in this study. One participant was excluded because markers had fallen off during the motion analysis. In total four men and six women were included. The participants had a mean age of 27.1 (SD 7.4) years, a mean length of 176.6 (SD 10.6) cm and a mean weight of 70.1 (SD 11.1) kg. The characteristics of each participant can be found in Appendix 2. All participants experienced no pain in the knees during activities of daily living, had no medical history of patellofemoral disorder and had no gait disturbances.

#### **3.2 Exploring the PFJCF estimation**

The difference in PFJCF between the static optimization method and inverse dynamics method is higher during stair descending, sit-to-stand and stand-to-sit than during walking and stair ascending (Figure 10, Appendix 9). This is best visible around the peak of the PFJCF. While the static optimization method resulted in higher PFJCF during walking, the inverse dynamics method resulted in higher PFJCF during stair ascending, stair descending, sit-to-stand and stand-to-sit. Gill's model resulted in higher PFJCF estimates compared to van Eijden's model and Yamaguchi's model during stair ascending, stair descending sit-to-stand and stand-to-sit, and in lower PFJCF estimates compared to van Eijden's model and Yamaguchi's model during walking. Van Eijden's model resulted in higher PFJCF estimates compared to Yamaguchi's model during stair ascending, stair descending sit-to-stand and stand-to-sit, and in lower PFJCF estimates compared to Yamaguchi's model during walking. The difference in PFJCF among the P2QFR models seems more or less equal between the quadriceps muscle force estimation methods. The PFJCF estimations will be further explored by analysing the peak PFJCF per activity.



- PFJCF van Eijden - ID method
- - - PFJCF van Eijden - SO method
- PFJCF Yamaguchi - ID method
- - - PFJCF Yamaguchi - SO method
- PFJCF Yamaguchi extrapolated
- PFJCF Gill - ID method
- - - PFJCF Gill - SO method

**Figure 10.** The estimated PFJCF in BW for each activity. The average PFJCF as a function of the percentage of the respective cycle is plotted. The PFJCF is averaged for each trial and for all participants (n=100).

### 3.3 Walking

Peak PFJCF using van Eijden's model, Yamaguchi's model and Gill's model was 0.46 BW, 0.47 BW and 0.42 BW, respectively for the inverse dynamics method and 0.56 BW, 0.57 BW and 0.51 BW, respectively for the static optimization method (Table 2, Appendix 10). The static optimization method resulted in a significantly higher peak PFJCF compared to the inverse dynamics method ( $p < 0.01$ ). The effect size for van Eijden's model, Yamaguchi's model and Gill's model was 0.10 BW, 0.10 BW and 0.09 BW, respectively (Table 2). The relative difference between the quadriceps muscle force estimation methods was largest for van Eijden's model, namely 9.8% (Table 3). Yamaguchi's model resulted in a significantly higher peak PFJCF compared to van Eijden's model and Gill's model ( $p < 0.01$ ). Also van Eijden's model resulted in a significantly higher peak PFJCF compared to Gill's model ( $p < 0.01$ ). The largest effect size was found between Yamaguchi's model and Gill's model using the static optimization method, namely 0.06 BW (Table 2). The relative difference among the P2QFR models was largest for Gill's model using both the inverse dynamics and static optimization method, namely 6.7% (Table 3). An interaction effect was found between type of quadriceps muscle force estimation method and type of P2QFR on the peak PFJCF estimation ( $P < 0.01$ ).

### 3.4 Stair ascending

Peak PFJCF using van Eijden's model, Yamaguchi's model and Gill's model was 3.53 BW, 3.51 BW and 3.66 BW, respectively for the inverse dynamics method and 3.45 BW, 3.44 BW and 3.57 BW, respectively for the static optimization method (Table 2, Appendix 10). The difference in peak PFJCF between the two quadriceps muscle force estimation methods was not significant ( $p > 0.05$ ). Gill's model resulted in a significantly higher peak PFJCF compared to van Eijden's model and Yamaguchi's model ( $p < 0.01$ ). The largest effect size was found between Yamaguchi's and Gill's model using the inverse dynamics methods, namely 0.15 BW (Table 2). The relative difference among the P2QFR models was largest for Gill's model using the inverse dynamics method, namely 2.6% (Table 3). No interaction effect was found between type of quadriceps muscle force method and type of P2QFR on the peak PFJCF estimation ( $P > 0.05$ ).

### 3.5 Stair descending

Peak PFJCF using van Eijden's model, Yamaguchi's model and Gill's model was 3.99 BW, 3.91 BW and 4.23 BW, respectively for the inverse dynamics method and 3.59 BW, 3.53 BW and

3.78 BW, respectively for the static optimization method (Table 2, Appendix 10). The inverse dynamics method resulted in a significantly higher peak PFJCF compared to the static optimization method ( $p < 0.01$ ). The effect size for van Eijden's model, Yamaguchi's model and Gill's model was 0.40 BW 0.38 BW and 0.45 BW, respectively (Table 2). The relative difference between the quadriceps muscle force estimation methods was largest for van Gill's model, namely 5.6% (Table 3). Gill's model resulted in a significantly higher peak PFJCF compared to van Eijden's model and Yamaguchi's model ( $p < 0.01$ ). Also, van Eijden's model resulted in a significantly higher peak PFJCF compared to Yamaguchi's model ( $p < 0.01$ ). The largest effect size was found between Yamaguchi's model and Gill's model using the inverse dynamics method, namely 0.32 BW (Table 2). The relative difference among the P2QFR models was largest for Gill's model using the inverse dynamics method, namely 4.6% (Table 3). An interaction effect was found between type of quadriceps muscle force method and type of P2QFR on the peak PFJCF estimation ( $p < 0.01$ ).

### **3.6 Sit-to-Stand**

Peak PFJCF using van Eijden's model, Yamaguchi's model and Gill's model was 4.07 BW, 3.98 BW and 4.70 BW, respectively for the inverse dynamics method and 3.07 BW, 3.00 BW and 3.53 BW, respectively for the static optimization method (Table 2, Appendix 10). The inverse dynamics method resulted in a significantly higher peak PFJCF compared to the static optimization method ( $p < 0.01$ ). The effect size for van Eijden's model, Yamaguchi's model and Gill's model was 1.00 BW, 0.98 BW and 1.17 BW, respectively (Table 2). The relative difference between the quadriceps muscle force estimation methods was largest for van Gill's model, namely 14.2% (Table 3). Gill's model resulted in a significantly higher peak PFJCF compared to van Eijden's model and Yamaguchi's model ( $p < 0.01$ ). The largest effect size was found between Yamaguchi's model and Gill's model using the inverse dynamics method, namely 0.72 BW. The relative difference among the P2QFR models was largest for Gill's model using the inverse dynamics method, namely 10.6% (Table 3). An interaction effect was found between type of quadriceps muscle force method and type of P2QFR on the peak PFJCF estimation ( $p < 0.01$ ).

### **3.7 Stand-to-Sit**

Peak PFJCF using van Eijden's model, Yamaguchi's model and Gill's model was 3.97 BW, 3.86 BW and 4.58 BW, respectively for the inverse dynamics method and 2.90 BW, 2.83 BW and

3.33 BW, respectively for the static optimization method (Table 2, Appendix 10). The inverse dynamics method resulted in a significantly higher peak PFJCF compared to the static optimization method ( $p < 0.01$ ). The effect size for van Eijden's model, Yamaguchi's model and Gill's model was 1.07 BW 1.03 BW and 1.25 BW, respectively (Table 2). The relative difference between the quadriceps muscle force estimation methods was largest for van Gill's model, namely 15.8% (Table 3). Gill's model resulted in a significantly higher peak PFJCF compared to van Eijden's model and Yamaguchi's model ( $p < 0.01$ ). The largest effect size was found between Yamaguchi's model and Gill's model during the inverse dynamics method, namely 0.72 BW. The relative difference among the P2QFR models was largest for Gill's model using the inverse dynamics method, namely 10.7% (Table 3). An interaction effect was found between type of quadriceps muscle force method and type of P2QFR on the peak PFJCF estimation ( $p < 0.01$ ).

**Table 2. Descriptive results of the peak PFJCF per activity.** The average peak PFJCF for each estimation method is summarized per activity. Also the absolute difference among methods is reported.

Walking		Peak PFJCF (BW)			Absolute difference in peak PFJCF (BW)		
Quadriceps force	P2QFR	Van Eijden	Yamaguchi	Gill	Van Eijden – Yamaguchi	Van Eijden – Gill	Yamaguchi – Gill
		<i>Inverse dynamics method (ID)</i>	0.46 (SD .25)	0.47 (SD .26)	0.42 (SD .24)	0.01	0.04
<i>Static optimization method (SO)</i>		0.56 (SD .27)	0.57 (SD .28)	0.51 (SD .26)	0.01	0.05	0.06
<b>Absolute difference in peak PFJCF (BW) ID – SO</b>		0.10	0.10	0.09			

Stair Ascending		Peak PFJCF (BW)			Absolute difference in peak PFJCF (BW)		
Quadriceps force	P2QFR	Van Eijden	Yamaguchi	Gill	Van Eijden – Yamaguchi	Van Eijden – Gill	Yamaguchi – Gill
		<i>Inverse dynamics method (ID)</i>	3.53 (SD .63)	3.51 (SD .61)	3.66 (SD .67)	0.02	0.13
<i>Static optimization method (SO)</i>		3.45 (SD .46)	3.44 (SD .43)	3.57 (SD .51)	0.01	0.12	0.13
<b>Absolute difference in peak PFJCF (BW) ID – SO</b>		0.08	0.07	0.09			

Stair Descending		Peak PFJCF (BW)			Absolute difference in peak PFJCF (BW)		
Quadriceps force	P2QFR	Van Eijden	Yamaguchi	Gill	Van Eijden – Yamaguchi	Van Eijden – Gill	Yamaguchi – Gill
		<i>Inverse dynamics method (ID)</i>	3.99 (SD .55)	3.91 (SD .53)	4.23 (SD .61)	0.08	0.24
<i>Static optimization method (SO)</i>		3.59 (SD .48)	3.53 (SD .47)	3.78 (SD .51)	0.06	0.19	0.25
<b>Absolute difference in peak PFJCF (BW) ID – SO</b>		0.40	0.38	0.45			

Sit-To-Stand	Peak PFJCF (BW)			Absolute difference in peak PFJCF (BW)		
	Van Eijden	Yamaguchi	Gill	Van Eijden - Yamaguchi	Van Eijden - Gill	Yamaguchi - Gill
Quadriceps force P2QFR						
Inverse dynamics method (ID)	4.07 (SD .79)	3.98* (SD .91)	4.70 (SD .98)	0.09	0.63	0.72
Static optimization method (SO)	3.07 (SD .62)	3.00* (SD .72)	3.53 (SD .75)	0.07	0.46	0.53
<b>Absolute difference in peak PFJCF (BW) ID - SO</b>	1.00	0.98	1.17			

Stand-To-Sit	Peak PFJCF (BW)			Absolute difference in peak PFJCF (BW)		
	Van Eijden	Yamaguchi	Gill	Van Eijden - Yamaguchi	Van Eijden - Gill	Yamaguchi - Gill
Quadriceps force P2QFR						
Inverse dynamics method (ID)	3.97 (SD .75)	3.86* (SD .83)	4.58 (SD .93)	0.11	0.61	0.72
Static optimization method (SO)	2.90 (SD .54)	2.83* (SD .61)	3.33 (SD .66)	0.07	0.43	0.50
<b>Absolute difference in peak PFJCF (BW) ID - SO</b>	1.07	1.03	1.25			

\*Based on the extrapolated curve of Yamaguchi's model.

**Table 3. The relative difference in peak PFJCF among the different biomechanical estimation methods.** The relative difference was described relative to the mean of the different estimation methods. In the left part of the table, the relative difference of the quadriceps muscle force estimation methods is described for each P2QFR model. In the right part of the table, the relative difference of the P2QFR models is described for each quadriceps muscle force estimation method.

Quadriceps muscle force estimation method		Relative difference (%)				
		Inverse dynamics	Static optimization	Van Eijden	Yamaguchi	Gill
<b>Walking</b>						
van Eijden	-9.8	9.8	Inverse dynamics	2.2	4.4	-6.7
Yamaguchi	-9.6	9.6	Static optimization	2.4	4.3	-6.7
Gill	-9.7	9.7				
<b>Stair Ascending</b>						
van Eijden	1.1	-1.1	Inverse dynamics	-1.0	-1.6	2.6
Yamaguchi	1.0	-1.0	Static optimization	-1.1	-1.3	2.4
Gill	1.2	-1.2				
<b>Stair descending</b>						
van Eijden	5.3	-5.3	Inverse dynamics	-1.3	-3.3	4.6
Yamaguchi	5.1	-5.1	Static optimization	-1.2	-2.8	4.0
Gill	5.6	-5.6				
<b>Sit-To-Stand</b>						
van Eijden	14.0	-14.0	Inverse dynamics	-4.2	-6.4	10.6
Yamaguchi	14.0	-14.0	Static optimization	-4.1	-6.3	10.3
Gill	14.2	-14.2				
<b>Stand-to-Sit</b>						
van Eijden	15.6	-15.6	Inverse dynamics	-4.0	-6.7	10.7
Yamaguchi	15.4	-15.4	Static optimization	-4.0	-6.3	10.3
Gill	15.8	-15.8				

## 4. Discussion

The purpose of this study was to explore how different biomechanical models of the patellofemoral joint affected the estimated PFJCF for common weight-bearing activities. This was done by performing biomechanical analyses based on motion analysis whereby marker trajectory data and force plate data were collected. From these data, the quadriceps muscle force was estimated twice, using the inverse dynamics method and static optimization method. Subsequently, P2QFRs, based on van Eijden's model, Yamaguchi's model and Gill's model, were used to estimate the PFJCF. The peak PFJCF was the extracted variable of interest.

It was hypothesized that the use of the static optimization method would result in higher peak PFJCF estimates compared to the use of the inverse dynamics method. Also it was hypothesized that above 60 degrees of knee flexion Gill's model would result in higher peak PFJCF compared to van Eijden's and Yamaguchi's model, and that van Eijden's model would result in higher peak PFJCF compared to Yamaguchi's model. Below 60 degrees it was hypothesized that Gills model would result in lower peak PFJCF compared to van Eijden's and Yamaguchi's model, and that van Eijden's model would result in lower peak PFJCF compared to Yamaguchi's model.

### 4.1 Clinical relevance

The magnitude of the difference in peak PFJCF was explored among the different estimation methods and it was determined whether the difference was statistically significant. Another way to evaluate the results is by discussing whether the difference in peak PFJCF is clinically relevant. In this way the practical importance of the difference can be determined.

Ideally the clinical relevance would be determined by comparing the difference in peak PFJCF that results in less pain experience in patients with the difference in peak PFJCF among different estimation methods. For example, if it is found that less pain is perceived during a task when the peak PFJCF is  $xx$  BW less during a certain period of time. And the difference in peak PFJCF between model A and B is higher than the  $xx$  BW, then the difference between the models is clinically relevant. Unfortunately, no such study was found. Therefore, the clinical relevance was determined by comparing the difference in peak PFJCF among the estimation models with the difference in peak PFJCF between healthy control groups and patellofemoral disease groups.

Three studies have been found that compared the peak PFJCF between a healthy control group and a patellofemoral disease group. Brechter and Powers (2002) compared the peak PFJCF between a healthy control group and PFP group during walking<sup>[40]</sup> and stair ascending<sup>[37]</sup>. Fok, Schache and Crossley (2013)<sup>[41]</sup> compared the peak PFJCF between a healthy control group and PFOA group during stair ascending and stair descending (Table 4). Also the biomechanical models used in these studies to estimate the quadriceps muscle force and PFJCF are reported. No studies were found that compared the peak PFJCF between a control group and a patellofemoral disease group during sit-to-stand and stand-to-sit.

**Table 4. In the literature reported peak PFJCF.** Reported peak PFJCF for healthy and patellofemoral disease groups for different weight-bearing-activities, including the absolute difference between the groups and the relative difference in peak PFJCF relative to the control group. *The standard deviation or 95% confidence interval is reported.*

Study	Activity	Population group	Quadriceps muscle force estimation method	PFJCF estimation based on model of	Peak PFJCF (BW)	Difference in peak PFJCF (BW)
<i>Brechter et al. (2002)</i> <sup>[40]</sup>	Free walking	Control	<i>inverse dynamics</i>	<i>van Eijden et al. (1986)</i> <sup>[27]</sup>	0.97 (SD 0.13)	0.21 (-21.6%)
		PFP			0.76 (SD 0.13)	
<i>Brechter et al. (2002)</i> <sup>[37]</sup>	Stair ascending	Control	<i>inverse dynamics</i>	<i>van Eijden et al. (1986)</i> <sup>[27]</sup>	3.84*	1.29 (-33.6%)
		PFP			2.55*	
<i>Fok, et al. (2013)</i> <sup>[41]</sup>	Stair ascending	Control	<i>static optimization</i>	<i>Buff et al. (1988)</i> <sup>[42]</sup>	2.15 CI [1.97 2.33]	0.54 (-25.1%)
		PFOA			1.61 CI [1.41 1.81]	
<i>Fok et al. (2013)</i> <sup>[41]</sup>	Stair descending	Control	<i>static optimization</i>	<i>Buff et al. (1988)</i> <sup>[42]</sup>	1.72 CI [1.43 2.01]	0.80 (-46.5%)
		PFOA			0.92 CI [0.59 1.24]	

\*No standard deviation or confidence interval was reported.

For free walking an absolute difference of 0.21 BW<sup>[40]</sup> in peak PFJCF was reported between a healthy control group and a PFP group. The largest difference in peak PFJCF among the different biomechanical estimation methods found in this study was around 0.10 BW, so approximately half the mean difference between controls and symptomatic patients.

For stair ascending an absolute difference of 1.29 BW<sup>[37]</sup> and 0.54 BW<sup>[41]</sup> in peak PFJCF was reported between a healthy control group and a PFP group. The largest difference in peak PFJCF among the different biomechanical estimation methods found in this study was 0.15 BW and therefore quite smaller.

For stair descending an absolute difference of 0.80 BW<sup>[41]</sup> in peak PFJCF was reported between a healthy control group and a patellofemoral osteoarthritis group. The largest difference in peak PFJCF among the different biomechanical estimation methods found in this study was 0.45 BW, so more than half the mean difference between controls and symptomatic patients.

Since the methods showed differences of half the size effect of the symptomatic patellofemoral population in walking and stair descending, it can be concluded that the model could significantly affect outcomes, and therefore mask clinical significant differences when results of different models are compared.

#### **4.2 Interpretation of quadriceps muscle force estimation methods**

For walking, the use of the static optimization method, for estimating quadriceps muscle force, resulted in a higher peak PFJCF estimation compared to the use of the inverse dynamics method. This finding is consistent with the hypothesis. However, for stair ascending, stair descending, sit-to-stand and stand-to-sit, the findings are inconsistent with the hypothesis; here the use of the static optimization method for estimating the quadriceps muscle force resulted in lower peak PFJCF estimations compared to the use of the inverse dynamics method.

The moment arm used to estimate the quadriceps muscle force directly from the knee extensor moment (the inverse dynamics method) differs from the moment arm used in the static optimization method (Figure 11). For the inverse dynamics method, a formula proposed by Brechter and Powers (2002)<sup>[37]</sup> (Equation 7) was used to describe the effective moment arm of the quadriceps muscle. By using the effective moment arm of the quadriceps muscle force both spacing and leveraging function of the patella are included. The same effective moment arm was used for all participants. For the static optimization method, the generic 2392 model was scaled to get participant-specific models. By doing so, also the general quadriceps moment arm of the 2392 model was scaled. Thus for each participant a participant-specific quadriceps moment arm was used. The difference in moment arm is an extra factor that has influenced the quadriceps muscle force estimation. Also, the fact that only the static optimization method used a participant-specific moment arm could have caused that the difference in peak PFJCF between the two quadriceps muscle force methods differed among the participants.

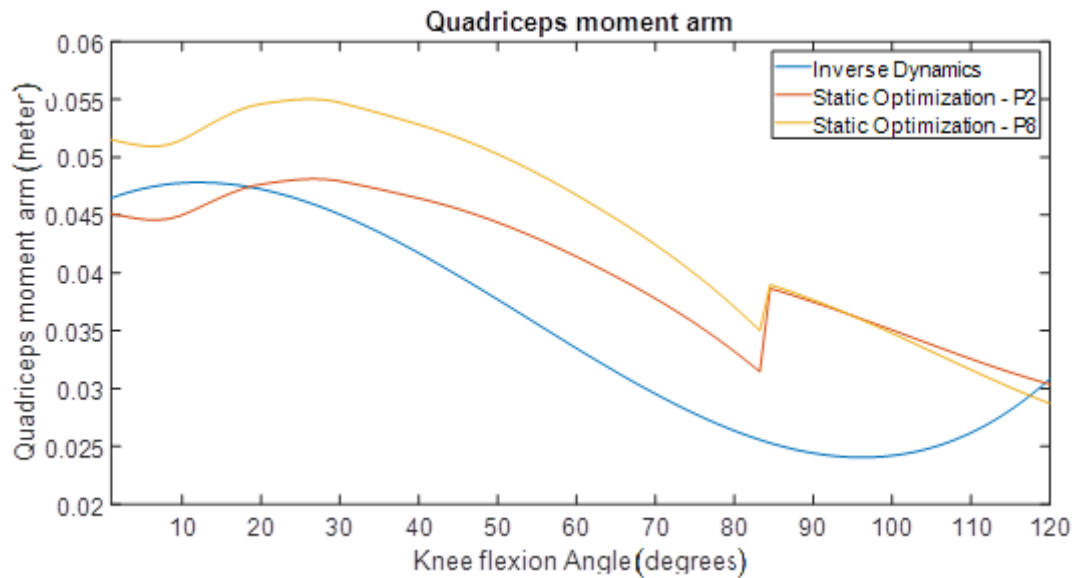


**Figure 12. Quadriceps moment arm used in the different estimation methods.** While in the inverse dynamics method one general moment arm is used, participant-specific moment arms are used in the static optimization method. For the static optimization method only the rectus femoris moment arm is plotted.

Differences between the inverse dynamics tool and static optimization tool may give another explanation for the unexpected results. To run the inverse dynamics tool of OpenSim, three input files are needed: the participant-specific musculoskeletal model, the experimentally measured ground reaction force data and the generalized coordinates estimated with the inverse kinematics tool. Marker errors, noise, differences between the participant-specific musculoskeletal model and the participant (e.g. geometry, inertial parameters, modelling assumptions) and other errors from the motion analysis lead to an inconsistency between the model accelerations, estimated from measured marker kinematics, and the experimentally measured ground reaction force data of the participant<sup>[36]</sup>. This dynamic inconsistency makes that Newton's second law is violated (Equation 11). The inverse dynamics tool applies residual forces and moments to the pelvis segment to account for this dynamic inconsistency. To run the static optimization tool, an extra input file is needed that contains residual actuators for each degree-of-freedom (Equation 12). It is possible that during static optimization the optimizers used more residual forces and therefore less muscle forces compared to the inverse dynamics method. This can explain why the static optimization resulted in lower quadriceps muscle forces and subsequently lower PFJCF compared to the inverse dynamics method in stair ascending, stair descending, sit-to-stand and stand-to-sit.

$$11 \quad \vec{F}_{exp} \neq m \cdot \vec{a}$$

$F_{exp}$  = experimentally measured ground reaction force,  $m$  = mass of the musculoskeletal model,  $a$  = model accelerations

$$12 \quad \vec{F}_{exp} + \vec{F}_{residual} = m \cdot \vec{a}$$

$F_{exp}$  = experimentally measured ground reaction force,  $F_{residual}$  = added residual forces  $m$  = mass of the musculoskeletal model,  $a$  = model

### 4.3 Interpretation of the P2QFRs

The biomechanical models influenced the estimated PFJCF in the way as was hypothesized by looking at their P2QFRs. The P2QFR depends on the quadriceps muscle force and knee flexion angle. Therefore, the knee flexion angle at which peak PFJCF occurred determines the difference in peak PFJCF among the biomechanical models. Table 5 summarizes the knee flexion angle at which the peak PFJCF occurred, for each estimation method and each activity. The peak PFJCF is different for each weight-bearing activity and therefore the effect of using different biomechanical models on the estimation of the PFJCF differs for the different weight-bearing activities.

**Table 5. Knee flexion angle at peak PFJCF.** For each estimation method the knee flexion angle at which the peak PFJCF occurred is summarized per weight-bearing activity.

Activity	Knee Flexion Angle (degrees)					
	Van Eijden SO	Van Eijden ID	Yamaguchi SO	Yamaguchi ID	Gill SO	Gill ID
Walking	15	16	15	16	15	16
Stair Ascending	61	61	60	60	61	61
Stair Descending	65	67	65	67	66	68
Sit-To-Stand	92	93	92	93	92	92
Stand-To-Sit	90	93	91	93	92	93

The mean values of the P2QFRs were used to develop functions that describe the ratios. Thus, the estimated PFJCF is based on the mean value of the P2QFRs. It would have been informative to also estimate the PFJCF based on 95% confidence interval values of the P2QFR, and to compare the peak PFJCF based on the minimum P2QFR value of one model with the peak PFJCF based on the maximum P2QFR value of another model when determining whether the use of different model resulted in a meaningful difference in peak PFJCF. However, only van Eijden's model presented the mean P2QFR plus standard deviation (Figure 12). Yamaguchi's model and Gill's model did not present any information about the standard deviation of the P2QFR. In Table 6 the peak PFJCF based on the mean P2QFR of van

Eijden’s model (used in this study), the peak PFJCF based on the – 1 SD P2QFR and the peak PFJCF based on the + 1 SD P2QFR are shown for each weight-bearing activity. Comparing the peak PFJCF resulted from the – 1 SD or + 1 SD P2QFR instead of the mean P2QFR influences the effect size. For example, comparing the peak PFJCF between van Eijden’s model and Gill’s model based on the mean P2QFR resulted in an effect size of .05 BW during walking (using the static optimization method). However, when the peak PFJCF was based on the + 1 SD P2QFR of van Eijden’s model, the effect size was 2.4 times higher (.12 BW).

**Table 6. Peak PFJCF in BW for each activity using van Eijden’s model.** The peak PFJCF based on the – 1 SD, mean and + 1 SD P2QFRs of van Eijden’s model for both the static optimization method and inverse dynamics method.

Van Eijden’s model	Peak PFJCF (BW)					
	Inverse dynamics			Static optimization		
	- 1 SD	mean	+ 1 SD	- 1 SD	mean	+ 1 SD
<b>Walking</b>	0.40	<b>0.46</b>	0.53	0.48	<b>0.56</b>	0.65
<b>Stair Ascending</b>	3.35	<b>3.53</b>	3.75	3.29	<b>3.45</b>	3.66
<b>Stair descending</b>	3.81	<b>3.99</b>	4.22	3.42	<b>3.59</b>	3.80
<b>Sit-To-Stand</b>	3.90	<b>4.07</b>	4.25	2.94	<b>3.06</b>	3.20
<b>Stand-to-Sit</b>	3.80	<b>3.97</b>	4.14	2.78	<b>2.90</b>	3.03

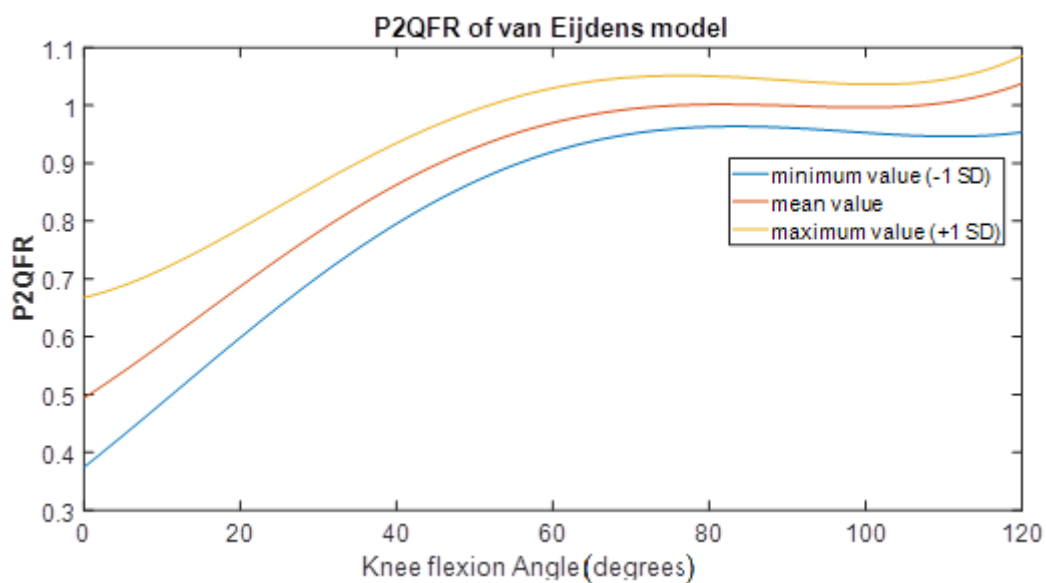


**Figure 13. Functions of the P2QFRs of van Eijden’s model.** Based on the – 1 SD, mean and + 1 SD P2QFR.

#### 4.4 Evaluation of the biomechanical models

The results of this study contributed by determining whether the use of different biomechanical models resulted in statistically and clinically different peak PFJCF estimates. The difference in peak PFJCF between the quadriceps muscle force estimation methods was clinically not relevant. However, for walking, the static optimization method resulted in a

significantly higher peak PFJCF compared to the inverse dynamics method. And for stair descending, sit-to-stand and stand to sit, the inverse dynamics method resulted in a significantly higher peak PFJCF compared to the static optimization method (Table 7). This indicates that the different quadriceps muscle force estimation methods should not be used interchangeably. Therefore, the estimation method that is most appropriate for estimating the quadriceps muscle force should be used. The static optimization method is, compared to the inverse dynamics method, more appropriate to estimate the quadriceps muscle force, as it accounts for muscle co-contractions. The activation level of the muscles, determined by the static optimization, can be compared to reported activation levels in the literature to determine the accuracy of the results. Ideally the static optimization should also be EMG informed, to account for participant-specific muscle activation<sup>[43]</sup>.

**Table 7. Summary of the statistical results.**

Activity	Statistical analysis			Interaction effect	
	Quadriceps muscle force estimation significant		P2QFR significant		
<b>Walking</b>	Yes	<i>Static optimization &gt; Inverse dynamics</i>	Yes	-Yamaguchi's model > van Eijden's model & Gill's model - van Eijden's model > Gill's model	Yes
<b>Stair Ascending</b>	No		Yes	- Gill's model > van Eijden's model & Yamaguchi's model	No
<b>Stair Descending</b>	Yes	<i>Inverse dynamics &gt; static optimization</i>	Yes	- Gill's model > van Eijden's model & Yamaguchi's model - van Eijden's model > Yamaguchi's model	Yes
<b>Sit-to-Stand</b>	Yes	<i>Inverse dynamics &gt; static optimization</i>	Yes	- Gill's model > van Eijden's model & Yamaguchi's model	Yes
<b>Stand-to-Sit</b>	Yes	<i>Inverse dynamics &gt; static optimization</i>	Yes	- Gill's model > van Eijden's model & Yamaguchi's model	Yes

The difference in peak PFJCF among the P2QFRs was clinically not relevant. However, statistically significant differences were found (Table 7). This indicates that the P2QFRs, based on different biomechanical models, should not be used interchangeably. The question remains which of the biomechanical models is more appropriate for estimating the PFJCF. This will be discussed per weight-bearing activity, because the effect of using different biomechanical models on the estimation of the PFJCF differs for the different weight-bearing activities.

For walking, Yamaguchi's model resulted in a significantly higher peak PFJCF compared to van Eijden's model and Gill's model, and van Eijden's model resulted in a significantly higher peak PFJCF compared to Gill's model. Van Eijden's model has the highest face validity as they

used a higher data sample in determining their anatomical model parameters compared to Yamaguchi's model and Gill's model, ten, one and four, respectively. Therefore, the P2QFR based on van Eijden's model has the highest face validity to estimate the PFJCF for walking.

For stair ascending, stair descending, sit-to-stand and stand-to-sit, Gill's model resulted in significantly higher peak PFJCF compared to van Eijden's model and Yamaguchi's model. And for stair descending van Eijden's model resulted in significantly higher peak PFJCF compared to Yamaguchi's model. The models of van Eijden and Gill have, compared to Yamaguchi's model, a higher face validity for higher knee flexion angles as they included tendofemoral contact. However, it seems that Gill's model overestimated the P2QFR above 60 degrees compared to experimental reference data from Miller, Murray and Gill (1997)<sup>[22]</sup>. Therefore, the P2QFR based on van Eijden's model has the highest face validity to estimate the PFJCF for stair ascending, stair descending, sit-to-stand and stand-to-sit.

#### **4.5 Limitations**

This study has several limitations. First, as previous discussed, the mean values of the P2QFRs were used to develop functions of the ratios. It would have been informative to also estimate the PFJCF based on 95% CI values of the P2QFR and to compare the peak PFJCF based on the minimum P2QFR value of one model with the peak PFJCF based on the maximum P2QFR value of another model. Second, for the inverse dynamics method the effective moment arm of the quadriceps muscle, determined by van Eijden et al. (1987)<sup>[38]</sup>, was used. For the static optimization method the quadriceps moment arm determined by the OpenSim software was used. The difference in used moment arm between the quadriceps muscle force estimation methods is an extra factor that has influenced the differences in the estimated PFJCF. Third, to examine the clinical relevance the difference in peak PFJCF among the different estimation methods was compared to the difference in peak PFJCF between healthy control groups and patellofemoral disease groups. In this way the difference between two extremes was used to determine the clinical relevance. It would have been informative to also determine the clinical relevance by comparing the difference in peak PFJCF among the different estimation methods with the difference in peak PFJCF that results in less perceived pain in a patellofemoral disease group.

#### 4.6 Recommendations

For a better understanding of the mechanical loading in the patellofemoral joint future research should also focus on the stress distribution in the joint. Furthermore, a future study can be conducted that determines the anatomical system parameters needed for the different mathematical models (from MRI). It would be informative to explore how the use of the same anatomical system parameters in different mathematical models affect the outcome measures of the models. In the discussed patellofemoral joint models, the PFJCF can only be extracted by the P2QFR. A patellofemoral model could be developed whereby the PFJCF can be extracted individually. Lastly, a standard method should be introduced to facilitate easy interpretation and to strive for the most accurate PFJCF estimation.

#### 5. Conclusion

This study explored how different biomechanical models of the patellofemoral joint affected the estimated PFJCF for common weight-bearing activities. It was found that the choice of a biomechanical model has a critical effect on the estimation of the magnitude of the PFJCF. Depending on which of the quadriceps muscle force estimation method was used, for walking, stair ascending, stair descending, sit-to-stand and stand-to-sit, the peak PFJCF differed as much 0.10 BW, 0.09 BW, 0.45 BW, 1.17 BW and 1.25 BW respectively. And depending on which of the P2QFR models was used, the peak PFJCF differed as much 0.06 BW, 0.15 BW, 0.32 BW, 0.72 BW and 0.72 BW respectively.

For walking, the static optimization method resulted in significantly higher peak PFJCF compared to the inverse dynamics method. And for stair descending, sit-to-stand and stand to sit, the inverse dynamics method resulted in significantly higher peak PFJCF compared to the static optimization method. For walking, Yamaguchi's model resulted in a significantly higher peak PFJCF compared to van Eijden's model and Gill's model, and van Eijden's model resulted in a significantly higher peak PFJCF compared to Gill's model. For stair ascending, stair descending, sit-to-stand and stand-to-sit, Gill's model resulted in significantly higher peak PFJCF compared to van Eijden's model and Yamaguchi's model. And for stair descending van Eijden's model resulted in significantly higher peak PFJCF compared to Yamaguchi's model.

For walking and stair descending, the methods showed differences of half the size effect of the symptomatic patellofemoral population. Therefore it can be concluded that the model could significantly affect outcomes, and therefore mask clinical significant differences when results of different models are compared.

## References

1. Nielen MMJ, H.K., Schermer TRJ, *Incidentie en prevalentie van gezondheidsproblemen in de Nederlandse huisartsenpraktijk in 2018*. Uit: Nivel Zorgregistraties eerste lijn [Internet]. 2019 [Laatst gewijzigd op 17-09-2019; geraadpleegd op 24-09-2019]. URL:[www.nivel.nl/nl/nivel-zorgregistraties-eerste-lijn/incidenties-en-prevalenties](http://www.nivel.nl/nl/nivel-zorgregistraties-eerste-lijn/incidenties-en-prevalenties), 2019.
2. Goldring, M.B. and S.R. Goldring, *Articular cartilage and subchondral bone in the pathogenesis of osteoarthritis*. Ann N Y Acad Sci, 2010. **1192**: p. 230-7.
3. van der Esch, M., J. Knoop, M. van der Leeden, R. Voorneman, M. Gerritsen, D. Reiding, S. Romviel, D.L. Knol, W.F. Lems, and J. Dekker, *Self-reported knee instability and activity limitations in patients with knee osteoarthritis: results of the Amsterdam osteoarthritis cohort*. Clinical rheumatology, 2012. **31**(10): p. 1505-1510.
4. Dekker, J., G.M. van Dijk, and C. Veenhof, *Risk factors for functional decline in osteoarthritis of the hip or knee*. Current opinion in rheumatology, 2009. **21**(5): p. 520-524.
5. Duncan, R., G. Peat, E. Thomas, L. Wood, E. Hay, and P. Croft, *Does isolated patellofemoral osteoarthritis matter?* Osteoarthritis Cartilage, 2009. **17**(9): p. 1151-5.
6. Duncan, R., G. Peat, E. Thomas, E. Hay, and P. Croft, *Incidence, progression and sequence of development of radiographic knee osteoarthritis in a symptomatic population*. Annals of the rheumatic diseases, 2011. **70**(11): p. 1944-1948.
7. Mazuca, S.A., K.D. Brandt, B.P. Katz, Y. Ding, K.A. Lane, and K.A. Buckwalter, *Risk factors for progression of tibiofemoral osteoarthritis: an analysis based on fluoroscopically standardised knee radiography*. Annals of the rheumatic diseases, 2006. **65**(4): p. 515-519.
8. Hinman, R. and K. Crossley, *Patellofemoral joint osteoarthritis: an important subgroup of knee osteoarthritis*. 2007.
9. HealthPages, *Structures of the knee*. Retrieved on November 14, 2018 from <https://www.healthpages.org/anatomy-function/knee-joint-structure-function-problems/>.
10. Powers, C.M., E. Witvrouw, I.S. Davis, and K.M. Crossley, *Evidence-based framework for a pathomechanical model of patellofemoral pain: 2017 patellofemoral pain consensus statement from the 4th International Patellofemoral Pain Research Retreat, Manchester, UK: part 3*. Br J Sports Med, 2017. **51**(24): p. 1713-1723.
11. Christoforakis, J.J. and R.K. Strachan, *Internal derangements of the knee associated with patellofemoral joint degeneration*. Knee Surgery, Sports Traumatology, Arthroscopy, 2005. **13**(7): p. 581-584.
12. Musumeci, G., *The effect of mechanical loading on articular cartilage*. 2016, Multidisciplinary Digital Publishing Institute.
13. Amoako, A.O. and G.G.A. Pujalte, *Osteoarthritis in young, active, and athletic individuals*. Clinical Medicine Insights: Arthritis and Musculoskeletal Disorders, 2014. **7**: p. CMAMD. S14386.
14. Arden, N. and M.C. Nevitt, *Osteoarthritis: Epidemiology*. Best Practice & Research Clinical Rheumatology, 2006. **20**(1): p. 3-25.
15. Lagerman, *A review of knee anatomy*. Retrieved on November 14, 2018 from <https://thenakedphysio.com/2014/09/22/the-challenge-of-knee-pain/>.
16. Yamaguchi, G.T. and F.E. Zajac, *A planar model of the knee joint to characterize the knee extensor mechanism*. J Biomech, 1989. **22**(1): p. 1-10.
17. Scuderi, *The Patella*. Springer-Verlag Berlin and Heidelberg GmbH & Co. K, 1995.
18. Aglietti, P. and P.P.M. Menchetti, *Biomechanics of the patellofemoral joint*, in *The patella*. 1995, Springer. p. 25-48.
19. Roos, P.E., N. Barton, and R.W.M. van Deursen, *Patellofemoral joint compression forces in backward and forward running*. Journal of Biomechanics, 2012. **45**(9): p. 1656-1660.
20. Loudon, J.K., *BIOMECHANICS AND PATHOMECHANICS OF THE PATELLOFEMORAL JOINT*. International Journal of Sports Physical Therapy, 2016. **11**(6): p. 820-830.

21. Powers, C.M., R.B. Souza, and J.P. Fulkerson, *Chapter 22 - Patellofemoral Joint*, in *Pathology and Intervention in Musculoskeletal Rehabilitation (Second Edition)*, D.J. Magee, et al., Editors. 2016, W.B. Saunders. p. 798-835.
22. Miller, R., D. Murray, H. Gill, J. O'Connor, and J. Goodfellow, *In vitro patellofemoral joint force determined by a non-invasive technique*. *Clinical Biomechanics*, 1997. **12**(1): p. 1-7.
23. Powers, C.M., Y.-J. Chen, I. Scher, and T.Q. Lee, *The influence of patellofemoral joint contact geometry on the modeling of three dimensional patellofemoral joint forces*. *Journal of Biomechanics*, 2006. **39**(15): p. 2783-2791.
24. Hefzy, M. and H. Yang, *A three-dimensional anatomical model of the human patello-femoral joint, for the determination of patello-femoral motions and contact characteristics*. *Journal of biomedical engineering*, 1993. **15**(4): p. 289-302.
25. van der Kooij, H., B. Koopman, and F. van der Helm, *Human Motion Control*. 2008.
26. Gill, H.S. and J.J. O'Connor, *Biarticulating two-dimensional computer model of the human patellofemoral joint*. *Clinical Biomechanics*, 1996. **11**(2): p. 81-89.
27. van Eijden, T.M.G.J., E. Kouwenhoven, J. Verburg, and W.A. Weijs, *A mathematical model of the patellofemoral joint*. *Journal of Biomechanics*, 1986. **19**(3): p. 219-229.
28. Reilly, D.T. and M. Martens, *Experimental analysis of the quadriceps muscle force and patello-femoral joint reaction force for various activities*. *Acta Orthopaedica Scandinavica*, 1972. **43**(2): p. 126-137.
29. Escamilla, R.F., G.S. Fleisig, N.Q. Zheng, J.E. Lander, S.W. Barrentine, J.R. Andrews, B.W. Bergemann, and C.T. Moorman, *Effects of technique variations on knee biomechanics during the squat and leg press*. *Medicine and Science in Sports and Exercise*, 2001. **33**(9): p. 1552-1566.
30. Simpson, K.J., E.G. Jameson, and S. Odum, *Estimated patellofemoral compressive forces and contact pressures during dance landings*. *Journal of applied biomechanics*, 1996. **12**(1): p. 1-14.
31. Cleather, D.J., J.E. Goodwin, and A.M.J. Bull, *Hip and knee joint loading during vertical jumping and push jerking*. *Clinical Biomechanics*, 2013. **28**(1): p. 98-103.
32. Documentation, O., *Gait 2392 and 2354 Models*. . Retrieved on August 26, 2019 from <https://simtk-confluence.stanford.edu:8443/display/OpenSim/Gait+2392+and+2354+Models>.
33. OpenSim, *Documentation Scaling*. Retrieved on August 26, 2019 from <https://simtk-confluence.stanford.edu:8443/display/OpenSim/Scaling>.
34. Delp, S.L., F.C. Anderson, A.S. Arnold, P. Loan, A. Habib, C.T. John, E. Guendelman, and D.G. Thelen, *OpenSim: open-source software to create and analyze dynamic simulations of movement*. *IEEE transactions on biomedical engineering*, 2007. **54**(11): p. 1940-1950.
35. OpenSim, *Documentation Inverse Dynamics*. Retrieved on August 26, 2019 from <https://simtk-confluence.stanford.edu:8443/display/OpenSim/Inverse+Dynamics>.
36. OpenSim, *Documentation Static Optimization*. Retrieved on August 26, 2019 from <https://simtk-confluence.stanford.edu:8443/display/OpenSim/Static+Optimization>.
37. Brechter, J.H. and C.M. Powers, *Patellofemoral joint stress during stair ascent and descent in persons with and without patellofemoral pain*. *Gait & Posture*, 2002. **16**(2): p. 115-123.
38. Van Eijden, T., W. Weijs, E. Kouwenhoven, and J. Verburg, *Forces acting on the patella during maximal voluntary contraction of the quadriceps femoris muscle at different knee flexion/extension angles*. *Cells Tissues Organs*, 1987. **129**(4): p. 310-314.
39. Nunes, G.S., R.S. Silva, A.F. dos Santos, R.A.S. Fernandes, F.V. Serrao, and M. de Noronha, *Methods to assess patellofemoral joint stress: A systematic review*. *Gait & Posture*, 2018. **61**: p. 188-196.
40. Brechter, J.H. and C.M. Powers, *Patellofemoral stress during walking in persons with and without patellofemoral pain*. *Medicine and Science in Sports and Exercise*, 2002. **34**(10): p. 1582-1593.

41. Fok, L.A., A.G. Schache, K.M. Crossley, Y.C. Lin, and M.G. Pandy, *Patellofemoral Joint Loading During Stair Ambulation in People With Patellofemoral Osteoarthritis*. *Arthritis and Rheumatism*, 2013. **65**(8): p. 2059-2069.
42. Buff, H.-U., L.C. Jones, and D.S. Hungerford, *Experimental determination of forces transmitted through the patello-femoral joint*. *Journal of Biomechanics*, 1988. **21**(1): p. 17-23.
43. Pizzolato, C., D.G. Lloyd, M. Sartori, E. Ceseracciu, T.F. Besier, B.J. Fregly, and M. Reggiani, *CEINMS: A toolbox to investigate the influence of different neural control solutions on the prediction of muscle excitation and joint moments during dynamic motor tasks*. *J Biomech*, 2015. **48**(14): p. 3929-36.
44. Harrington, M.E., A.B. Zavatsky, S.E. Lawson, Z. Yuan, and T.N. Theologis, *Prediction of the hip joint centre in adults, children, and patients with cerebral palsy based on magnetic resonance imaging*. *J Biomech*, 2007. **40**(3): p. 595-602.

## Appendices

- Appendix 1 Patellofemoral Joint Models
- Appendix 2 Participant Characteristics
- Appendix 3 Informed Consent Form
- Appendix 4 Marker List
- Appendix 5 List of Virtual Created Markers
- Appendix 6 Individual Scaling Factors
- Appendix 7 Marker weights
- Appendix 8 P2QFR
- Appendix 9 Plots of the estimated PFJCF
- Appendix 10 Descriptive results of the peak PFJCF
- Appendix 11 Abbreviations
- Appendix 12 List of Figures, Tables and Equations

Appendix 1 Patellofemoral Joint Models

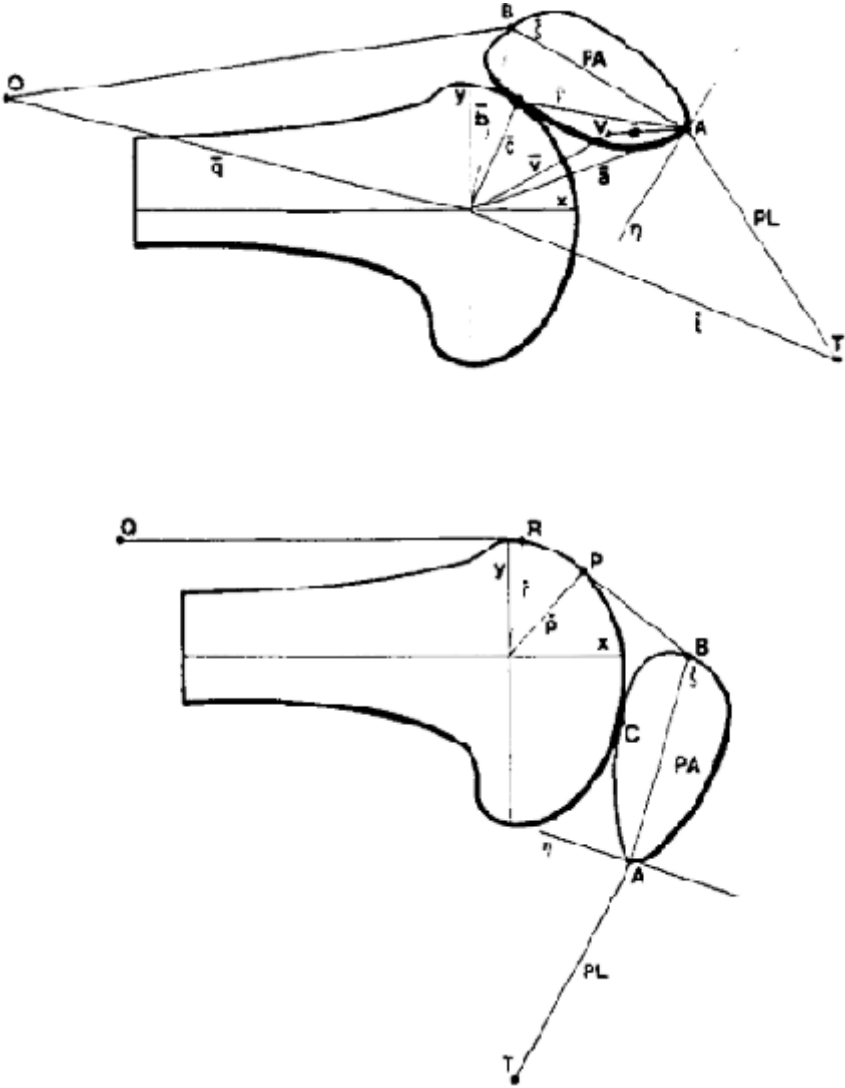


Figure A 1. Two-dimensional model of the patellofemoral joint from van Eijden et al. (1986)<sup>[27]</sup>. Upper panel: knee extension. Lower panel: high knee flexion. *Reproduced from van Eijden et al. (1986)<sup>[27]</sup>*

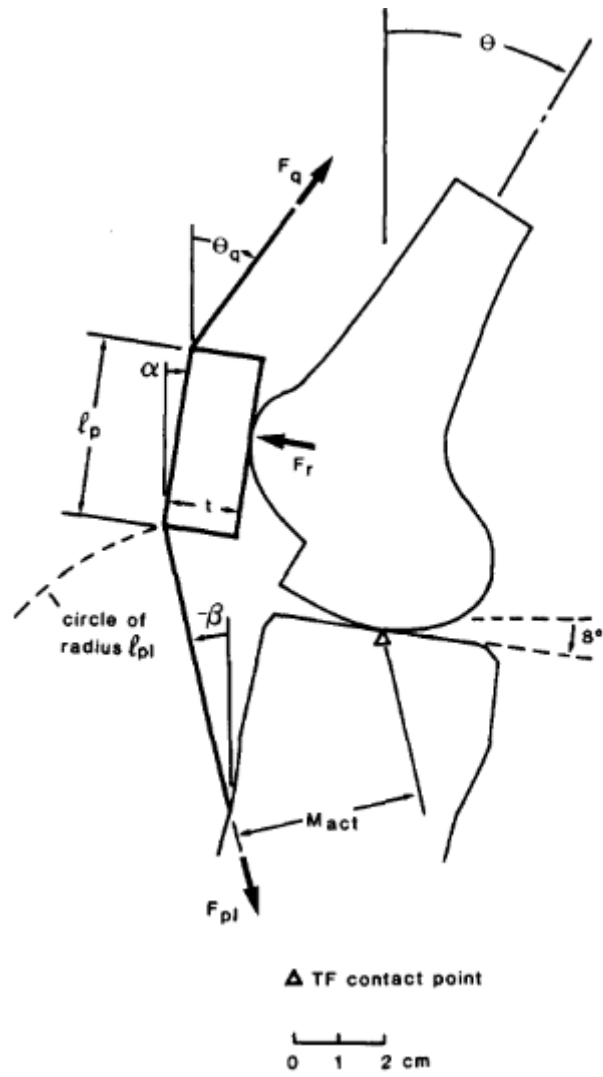


Figure A 2. Two-dimensional model of the patellofemoral joint from Yamaguchi et al. (1989)<sup>[16]</sup>. Reproduced from Yamaguchi et al. (1989)<sup>[16]</sup>

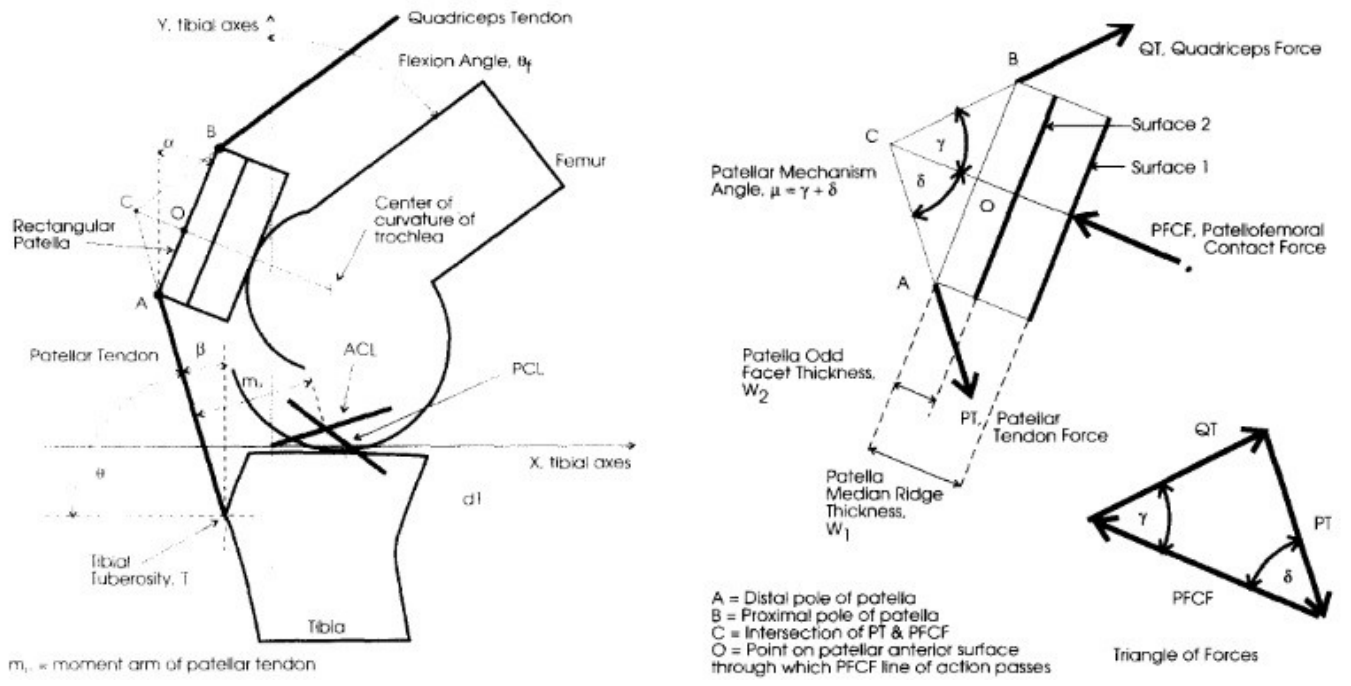


Figure A 3. Two-dimensional model of the patellofemoral joint from Gill et al. (1996)<sup>[26]</sup>. Left panel: Sagittal plane view of the knee. Right panel: Rectangular representation of the patella in sagittal plane. Reproduced from Gill et al. (1996)<sup>[26]</sup>.

## Appendix 2 Participant Characteristics

Table A1. Individual participant characteristics.

Participant	Gender	Age (years)	Length (cm)	Weight (kg)
1	F	27	168.9	79.0
2	F	25	170.4	61.7
3	F	25	174.7	61.9
4	M	25	192.5	72.9
5	F	48	164.4	60.4
6	F	24	169.1	66.1
7	F	25	175.3	66.9
8	M	23	194.5	95.5
9	M	25	169.9	60.6
10	M	24	186.2	76.2

## Appendix 3 Informed Consent Form

### Consent Form for Patellofemoral joint contact forces during weight-bearing activities: a direct comparison of different estimation methods.

*Please tick the appropriate boxes*

Yes No

#### **Taking part in the study**

I have read and understood the study information dated [ / / ], or it has been read to me. I have been able to ask questions about the study and my questions have been answered to my satisfaction.

I consent voluntarily to be a participant in this study and understand that I can refuse to answer questions and I can withdraw from the study at any time, without having to give a reason.

I understand that taking part in the study involves capture of motion analysis data and pictures of marker placement that will be stored in data files.

#### **Risks associated with participating in the study**

I understand that taking part in the study involves the following risks:

Participants might experience temporary redness and irritation of the skin caused by the tape used to apply the markers to the skin

Participants might experience an uncomfortable feeling while performing the tasks due to the dress code.

#### **Use of the information in the study**

I understand that information I provide will be used for a master thesis report and a possible publication.

I understand that personal information collected about me that can identify me, such as my name or medical history, will not be shared beyond the study team.

#### **Future use and reuse of the information by others**

I give permission for the motion analysis data that I provide to be archived on a secured server so it can be used for future research and learning.

I give permission for the personal data that I provide to be archived anonymously on a secured server so it can be used for future research and learning.

## Signatures

\_\_\_\_\_  
Name of participant                      Signature                      Date

I have accurately read out the information sheet to the potential participant and, to the best of my ability, ensured that the participant understands to what they are freely consenting.

## **Chantal Eenkhoorn**

\_\_\_\_\_  
Researcher name                      Signature                      Date

Study contact details for further information:

Chantal Eenkhoorn<sup>1</sup>, ([c.eenkhoorn@student.tudelft.nl](mailto:c.eenkhoorn@student.tudelft.nl))

<sup>1</sup> Master student, Biomedical Engineering, TU Delft

**Information sheet for participants in scientific research.**

---

**Project title: Patellofemoral joint contact forces during weight-bearing activities: a direct comparison of different estimation methods.**

---

Please take time to read the following information carefully. Ask questions if anything you read is not clear or if you would like more information.

**Purpose of the research project**

This research project is conducted to directly compare different methods of estimating patellofemoral joint contact forces during weight-bearing activities (walking, stair ambulation and sit-to-stand).

**Global design of the research**

The experiment will take place in the BioMechaMotion Lab at the TU delft. A motion capture system will be used to obtain kinematics and kinetics of the human body during walking, stair ambulation and a sit-to-stand exercise. For this study you are asked to wear shorts, so markers can be placed on both legs. It might be necessary to roll up your shirt to ensure that the markers placed on the hips are visible for the camera's. Double adhesive medical tape will be used to attach the markers to the skin. During the experiment you are asked to perform the following tasks: walking, stair ambulation and rising from a chair. You are also asked to fill out a questionnaire about some personal information i.e. name, date of birth, gender, weight, length, history of knee trauma or knee pain. A photo will be taken of the marker placement. This photo will be used to create a participant-specific lower extremity model. The experiment will take no longer than two hours.

**Possible risks**

Participating in this research is not anticipated to cause you any mental or physical harm. Participants with sensitive skin might experience temporary redness and irritation caused by the medical tape used to apply the markers. Please inform the researcher immediately if you feel any skin irritation or discomfort during the experiment.

**Data confidentiality**

The collected personal data will be used for research purposes only and will only be available to the researchers. All data will be anonymised in any publication. The participant has the right to request access to his/her own personal data for rectification or erasure.

**Ethical approval**

This research project has been ethically approved by the Human Research Ethics Committee (HREC) of the TU Delft.

**Right to withdraw**

The participant reserves the right to withdraw at any time without giving reasons.

**Contact for further information**

For any contact, further information or complaints, please use the following contact details.

Chantal Eenkhoorn<sup>1</sup>, ([c.eenkhoorn@student.tudelft.nl](mailto:c.eenkhoorn@student.tudelft.nl))

<sup>1</sup> Master student, Biomedical Engineering, TU Delft

Thank you for taking part in this research!

## **Questionnaire**

*To be completed by the participant:*

**Name:**

**Date of Birth:**

**Gender:**

**Do you have a history or diagnose of knee pathology or trauma?**

**Do you have knee pain during activities of daily living?**

**Do you have any medical disorders that affect your gait?**

---

*To be completed by the researcher:*

**Weight:**

**Length:**

**Circumference thigh right:**

**Circumference thigh left:**

**Circumference shank right:**

**Circumference shank left:**

**Circumference foot right:**

**Circumference foot left:**

**Length foot right:**

**Length foot left:**

## Appendix 4 Marker List

**Table A2. Marker list.** All markers per segment are listed. Also there label name is given and it is indicated whether it is an anatomical marker or tracking marker.

Segment	Position on the participant	Marker label	Marker type	
<b>Pelvis</b>	Right anterior superior iliac spine	ASIS_R	<i>Anatomical+Tracking</i>	
	Left anterior superior iliac spine	ASIS_L	<i>Anatomical+Tracking</i>	
	Right posterior superior iliac spine	PSIS_R	<i>Anatomical+Tracking</i>	
	Left posterior superior iliac spine	PSIS_L	<i>Anatomical+Tracking</i>	
	Sacral (midway between PSIS)	SACR	<i>Tracking</i>	
<b>Thigh</b>	Right Femur Condyle Lateral	FCL_R	<i>Anatomical+Tracking</i>	
	Left Femur Condyle Lateral	FCL_L	<i>Anatomical+Tracking</i>	
	Right Femur Condyle Medial	FCM_R	<i>Anatomical</i>	
	Left Femur Condyle Medial	FCM_L	<i>Anatomical</i>	
	Right Thigh Anterior Proximal	TAP_R	<i>Tracking</i>	
	Left Thigh Anterior Proximal	TAP_L	<i>Tracking</i>	
	Right Thigh Anterior Distal	TAD_R	<i>Tracking</i>	
	Left Thigh Anterior Distal	TAD_L	<i>Tracking</i>	
	Right Thigh Lateral Distal	TLD_R	<i>Tracking</i>	
	Left Thigh Lateral Distal	TLD_L	<i>Tracking</i>	
	Right Thigh Posterior Proximal	TPP_R	<i>Tracking</i>	
	Left Thigh Posterior Proximal	TPP_L	<i>Tracking</i>	
	Right Thigh Posterior Distal	TPD_R	<i>Tracking</i>	
	Left Thigh Posterior Distal	TPD_L	<i>Tracking</i>	
	<b>Shank</b>	Right Malleolus Lateral	ML_R	<i>Anatomical+Tracking</i>
Left Malleolus Lateral		ML_L	<i>Anatomical+Tracking</i>	
Right Malleolus Medial		MM_R	<i>Anatomical</i>	
Left Malleolus Medial		MM_L	<i>Anatomical</i>	
Right Caput Fibulae		CF_R	<i>Tracking</i>	
Left Caput Fibulae		CF_L	<i>Tracking</i>	
Right Tuberositas Tibia		TT_R	<i>Tracking</i>	
Left Tuberositas Tibia		TT_L	<i>Tracking</i>	
Right Shank anterior proximal		SAP_R	<i>Tracking</i>	
Left Shank anterior proximal		SAP_L	<i>Tracking</i>	
Right Shank anterior distal		SAD_R	<i>Tracking</i>	
Right Shank anterior distal		SAD_L	<i>Tracking</i>	
<b>Foot</b>		Right caput Metatarsale 1	CM1_R	<i>Anatomical+Tracking</i>
		Left caput Metatarsale 1	CM1_L	<i>Anatomical+Tracking</i>
		Right caput Metatarsale 5	CM5_R	<i>Anatomical+Tracking</i>
	Left caput Metatarsale 5	CM5_L	<i>Anatomical+Tracking</i>	
	Right posterior Calcaneus ( <i>height of CM5</i> )	CAL_R	<i>Anatomical+Tracking</i>	
	Left posterior Calcaneus ( <i>height of CM5</i> )	CAL_L	<i>Anatomical+Tracking</i>	
	Right Sustentaculum tali	STL_R	<i>Tracking</i>	
Left Sustentaculum tali	STL_L	<i>Tracking</i>		

## Appendix 5 List of Virtual Created Markers

**Table A3. List of virtual created markers.** These virtual created markers were used to scale the generic 2392 gait model of OpenSim into participant-specific models.

Segment	Position of the Marker	Marker Label
<b>Pelvis</b>	In the middle of the ASIS_R and ASIS_L markers	ASIS_MID
	In the middle of the PSIS_R and PSIS_L markers	PSIS_MID
	In the middle of the ASIS_MID and PSIS_MID markers	PELVIS_MID
<b>Thigh</b>	Right Hip Joint Center*	HJC_R
	Left Hip Joint Center*	HJC_L
	In the middle of the HJC_R and HJC_L	HJC_MID
<b>Shank</b>	In the middle of the FCM_R and FCL_R	KJC_R
	In the middle of the FCM_L and FCL_L	KJC_L
	In the middle of the MM_R and ML_R markers	AJC_R
	In the middle of the MM_R and ML_R markers	AJC_L
<b>Foot</b>	Projection of the AJC_R on the ground	P_AJC_R
	Projection of the AJC_L on the ground	P_AJC_L
	Projection of the CAL_R on the ground	P_CAL_R
	Projection of the CAL_L on the ground	P_CAL_L
	Projection of the CM5_R on the ground	P_CM5_R
	Projection of the CM5_L on the ground	P_CM5_L
	Projection of the CM1_R on the ground	P_CM1_R
	Projection of the CM1_L on the ground	P_CM1_L
	Projection of the middle of the CM5_R and CM1_R markers on the ground	P_MID-CM_R
	Projection of the middle of the CM5_R and CM1_R markers on the ground	P_MID-CM_L

\* estimated using the regression equation of Harrington, Zavatsky and Lawson (2007)<sup>[44]</sup>

## Appendix 6 Individual Scaling Factors

Table A4. List of individual scaling factors

Participant 1		Scale factor		
Segment	anterior/posterior	superior/inferior	medial/lateral	
<b>Pelvis</b>	0.933650	1.164338	1.383189	
<b>Femur right</b>	1.488200	1.039693	1.488200	
<b>Tibia right</b>	0.969943	0.997791	0.969943	
<b>Talus right</b>	1.015992	0.935119	1.187478	
<b>Calcaneus right</b>	1.015992	0.935119	1.187478	
<b>Toes right</b>	1.015992	0.935119	1.187478	
<b>Femur left</b>	1.516329	1.046006	1.516329	
<b>Tibia left</b>	0.966823	1.001905	0.966823	
<b>Talus left</b>	1.145027	0.872099	1.173407	
<b>Calcaneus left</b>	1.145027	0.872099	1.173407	
<b>Toes left</b>	1.145027	0.872099	1.173407	
<b>Torso</b>	1	1	1	

Participant 2		Scale factor		
Segment	anterior/posterior	superior/inferior	medial/lateral	
<b>Pelvis</b>	1.112028	0.888941	0.975893	
<b>Femur right</b>	1.318337	1.119631	1.318337	
<b>Tibia right</b>	0.905222	0.998667	0.905222	
<b>Talus right</b>	1.005111	1.000893	1.069111	
<b>Calcaneus right</b>	1.005111	1.000893	1.069111	
<b>Toes right</b>	1.005111	1.000893	1.069111	
<b>Femur left</b>	1.305508	1.101869	1.305508	
<b>Tibia left</b>	0.953635	1.013896	0.953635	
<b>Talus left</b>	1.171761	0.938015	1.062219	
<b>Calcaneus left</b>	1.171761	0.938015	1.062219	
<b>Toes left</b>	1.171761	0.938015	1.062219	
<b>Torso</b>	1	1	1	

Participant 3		Scale factor	
Segment	anterior/posterior	superior/inferior	medial/lateral
<b>Pelvis</b>	0.981024	0.904798	1.038085
<b>Femur right</b>	1.360845	1.105678	1.360845
<b>Tibia right</b>	0.964287	1.002267	0.964287
<b>Talus right</b>	1.061227	0.942862	1.264647
<b>Calcaneus right</b>	1.061227	0.942862	1.264647
<b>Toes right</b>	1.061227	0.942862	1.264647
<b>Femur left</b>	1.370203	1.069007	1.370203
<b>Tibia left</b>	0.991046	1.066036	0.991046
<b>Talus left</b>	1.147108	0.889269	1.287935
<b>Calcaneus left</b>	1.147108	0.889269	1.287935
<b>Toes left</b>	1.147108	0.889269	1.287935
<b>Torso</b>	1	1	1

Participant 4		Scale factor	
Segment	anterior/posterior	superior/inferior	medial/lateral
<b>Pelvis</b>	1.021565	0.884821	0.998046
<b>Femur right</b>	1.428272	1.203891	1.428272
<b>Tibia right</b>	1.048136	1.122661	1.048136
<b>Talus right</b>	1.166323	1.080592	1.227763
<b>Calcaneus right</b>	1.166323	1.080592	1.227763
<b>Toes right</b>	1.166323	1.080592	1.227763
<b>Femur left</b>	1.434149	1.198280	1.434149
<b>Tibia left</b>	1.036530	1.121608	1.036530
<b>Talus left</b>	1.229687	1.058198	1.260901
<b>Calcaneus left</b>	1.229687	1.058198	1.260901
<b>Toes left</b>	1.229687	1.058198	1.260901
<b>Torso</b>	1	1	1

Participant 5		Scale factors	
Segment	anterior/posterior	superior/inferior	medial/lateral
<b>Pelvis</b>	1.069781	0.980661	1.123548
<b>Femur right</b>	1.347696	0.984315	1.347696
<b>Tibia right</b>	0.956436	0.986210	0.956436
<b>Talus right</b>	1.027160	0.823687	1.078248
<b>Calcaneus right</b>	1.027160	0.823687	1.078248
<b>Toes right</b>	1.027160	0.823687	1.078248
<b>Femur left</b>	1.380495	0.999878	1.380495
<b>Tibia left</b>	0.933835	0.998978	0.933835
<b>Talus left</b>	1.134751	0.758786	1.070914
<b>Calcaneus left</b>	1.134751	0.758786	1.070914
<b>Toes left</b>	1.134751	0.758786	1.070914
<b>Torso</b>	1	1	1

Participant 6		Scale factor	
Segment	anterior/posterior	superior/inferior	medial/lateral
<b>Pelvis</b>	1.098058	0.967733	1.096565
<b>Femur right</b>	1.386660	0.994368	1.386660
<b>Tibia right</b>	0.996248	1.028073	0.996248
<b>Talus right</b>	1.036375	1.025702	1.162566
<b>Calcaneus right</b>	1.036375	1.025702	1.162566
<b>Toes right</b>	1.036375	1.025702	1.162566
<b>Femur left</b>	1.360887	0.990310	1.360887
<b>Tibia left</b>	0.989739	1.016651	0.989739
<b>Talus left</b>	1.107635	0.985311	1.229796
<b>Calcaneus left</b>	1.107635	0.985311	1.229796
<b>Toes left</b>	1.107635	0.985311	1.229796
<b>Torso</b>	1	1	1

Participant 7		Scale factors	
Segment	anterior/posterior	superior/inferior	medial/lateral
<b>Pelvis</b>	1.035918	0.928792	1.057837
<b>Femur right</b>	1.398355	0.994314	1.398355
<b>Tibia right</b>	0.965054	1.007331	0.965054
<b>Talus right</b>	0.996648	0.944529	1.010069
<b>Calcaneus right</b>	0.996648	0.944529	1.010069
<b>Toes right</b>	0.996648	0.944529	1.010069
<b>Femur left</b>	1.417915	0.984312	1.417915
<b>Tibia left</b>	0.978386	1.004730	0.978386
<b>Talus left</b>	1.086609	0.940268	1.142447
<b>Calcaneus left</b>	1.086609	0.940268	1.142447
<b>Toes left</b>	1.086609	0.940268	1.142447
<b>Torso</b>	1	1	1

Participant 8		Scale factor	
Segment	anterior/posterior	superior/inferior	medial/lateral
<b>Pelvis</b>	1.101518	1.027787	1.182545
<b>Femur right</b>	1.281712	1.253982	1.281712
<b>Tibia right</b>	1.042615	1.140588	1.042615
<b>Talus right</b>	1.094661	1.135284	1.337286
<b>Calcaneus right</b>	1.094661	1.135284	1.337286
<b>Toes right</b>	1.094661	1.135284	1.337286
<b>Femur left</b>	1.293100	1.234432	1.293100
<b>Tibia left</b>	1.048405	1.167117	1.048405
<b>Talus left</b>	1.219744	1.090635	1.347622
<b>Calcaneus left</b>	1.219744	1.090635	1.347622
<b>Toes left</b>	1.219744	1.090635	1.347622
<b>Torso</b>	1	1	1

Participant 9 Segment	Scale factor		
	anterior/posterior	superior/inferior	medial/lateral
<b>Pelvis</b>	0.919478	0.852638	0.979058
<b>Femur right</b>	1.181297	1.103497	1.181297
<b>Tibia right</b>	0.974886	0.932875	0.974886
<b>Talus right</b>	1.006823	0.990123	1.244369
<b>Calcaneus right</b>	1.006823	0.990123	1.244369
<b>Toes right</b>	1.006823	0.990123	1.244369
<b>Femur left</b>	1.233268	1.105604	1.233268
<b>Tibia left</b>	1.015130	0.958231	1.015130
<b>Talus left</b>	1.222595	0.937600	1.138969
<b>Calcaneus left</b>	1.222595	0.937600	1.138969
<b>Toes left</b>	1.222595	0.937600	1.138969
<b>Torso</b>	1	1	1

Participant 10 Segment	Scale factor		
	anterior/posterior	superior/inferior	medial/lateral
<b>Pelvis</b>	1.040534	0.932898	1.062407
<b>Femur right</b>	1.343028	1.156445	1.343028
<b>Tibia right</b>	1.065323	1.062940	1.065323
<b>Talus right</b>	1.114061	1.164527	1.340808
<b>Calcaneus right</b>	1.114061	1.164527	1.340808
<b>Toes right</b>	1.114061	1.164527	1.340808
<b>Femur left</b>	1.339288	1.160703	1.339288
<b>Tibia left</b>	1.092217	1.057667	1.092217
<b>Talus left</b>	1.162084	1.116987	1.307653
<b>Calcaneus left</b>	1.162084	1.116987	1.307653
<b>Toes left</b>	1.162084	1.116987	1.307653
<b>Torso</b>	1	1	1

## Appendix 7 Marker weights

Table A5. Marker weights. Used during the inverse kinematics step.

Marker label	Weight
ASIS_R	5
ASIS_L	5
PSIS_R	5
PSIS_L	5
FCL_R	10
FCL_L	10
CAL_R	10
CAL_L	10
ML_R	10
ML_L	10
CM5_R	10
CM5_L	10
CM1_R	10
CM1_L	10
HJC_R	20
HJC_L	20

## Appendix 8 P2QFR

Yamaguchi et al. (1989) <sup>[16]</sup>

Data points extracted from the PFJCF to quadriceps muscle force graph of Yamaguchi et al. The GRABIT function in Matlab software was used (mean of three data sets)

**Table A6. Digitized data points of Yamaguchi's model**

Knee flexion	0°	10°	20°	30°	40°	50°	60°	70°	80°	90°
<b>P2QFR</b>	.49	.60	.71	.81	.89	.95	.96	.96	.96	.96

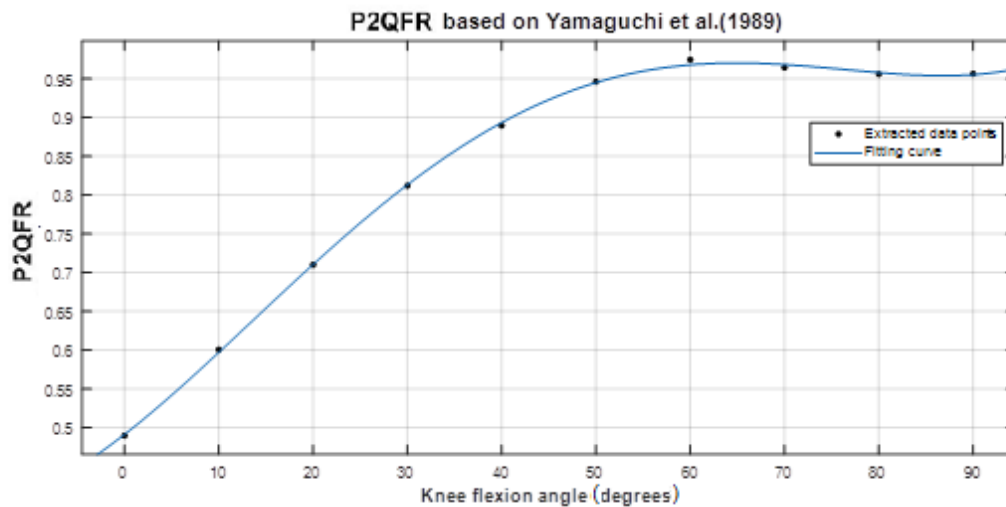


**Figure A 4. P2QFR based on Yamaguchi et al. (1989)** <sup>[16]</sup>

$$P2QFR = 0.21e^{-1}\theta^4 - 2.77e^{-5}\theta^3 - 0.14\theta^2 + 0.16\theta + 0.92$$

- Where  $\theta$  is normalized by mean 45 and std 30.28

Goodness of fit:

SSE:  $9.711e^{-5}$

R-square: 0.9996

Adjusted R-square: 0.9994

RMSE: 0.004407

Gill et al. (1996) <sup>[26]</sup>

Data points extracted from the PFJCF to quadriceps muscle force graph of Yamaguchi et al. The GRABIT function in Matlab software was used (mean of three data sets)

Table A7. Digitized data points of Gill's model.

Knee flexion	0°	10°	20°	30°	40°	50°	60°	70°	80°	90°	100°	110°	120°	130°	140°
P2QFR	.37	.51	.63	.75	.85	.93	1.00	1.06	1.10	1.12	1.18	1.19	1.18	1.16	1.13

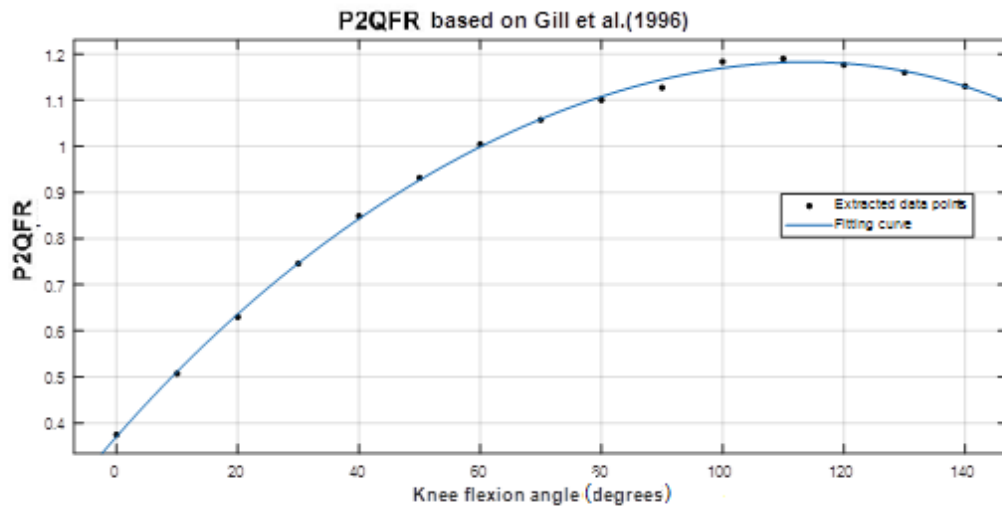


Figure A 5. P2QFR based on Gill et al. (1996) <sup>[26]</sup>

$$P2QFR = -0.44e^{-2\theta^4} - 4.55e^{-4\theta^3} - 0.12\theta^2 + 0.24\theta + 1.06$$

- Where  $\theta$  is normalized by mean 70 and std 44.72

Goodness of fit:

SSE: 0.0008081

R-square: 0.9992

Adjusted R-square: 0.9989

RMSE: 0.008989

## Appendix 9 Plots of the estimated PFJCF

### Walking

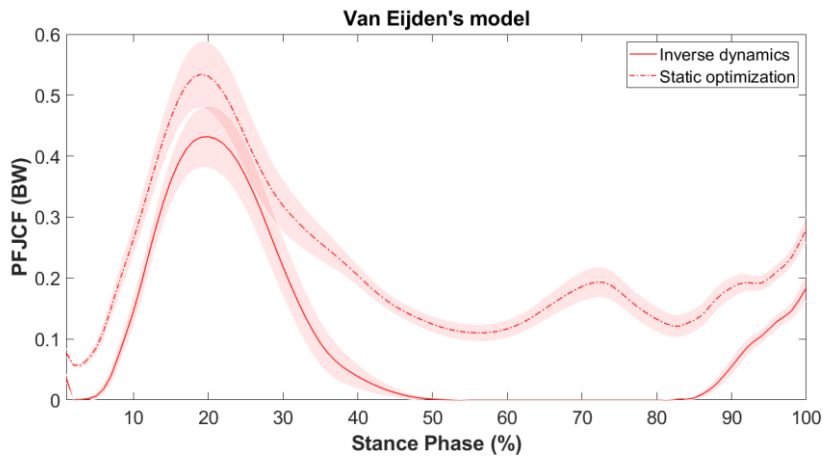


Figure A 6. PFJCF estimated using van Eijden's model during walking. PFJCF estimated using the inverse dynamics method and static optimization method. The 95% confidence interval of the mean is plotted. The PFJCF is averaged for each trial and for all participants (n=100).

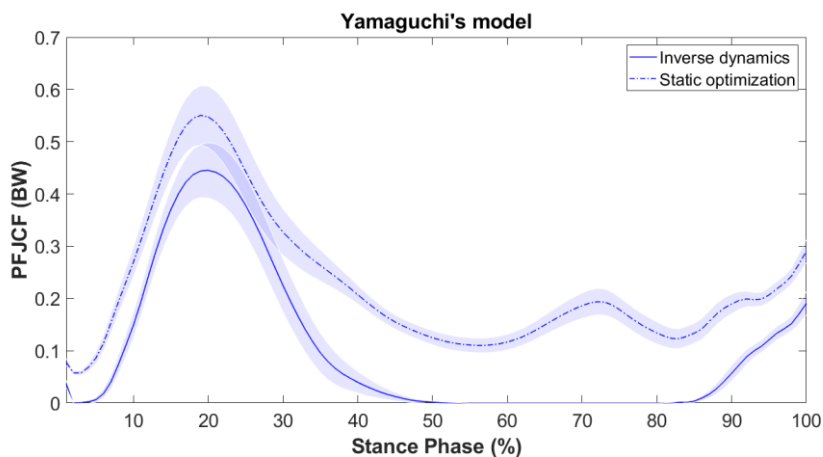


Figure A 7. PFJCF estimated using Yamaguchi's model during walking. PFJCF estimated using the inverse dynamics method and static optimization method. The 95% confidence interval of the mean is plotted. The PFJCF is averaged for each trial and for all participants (n=100).

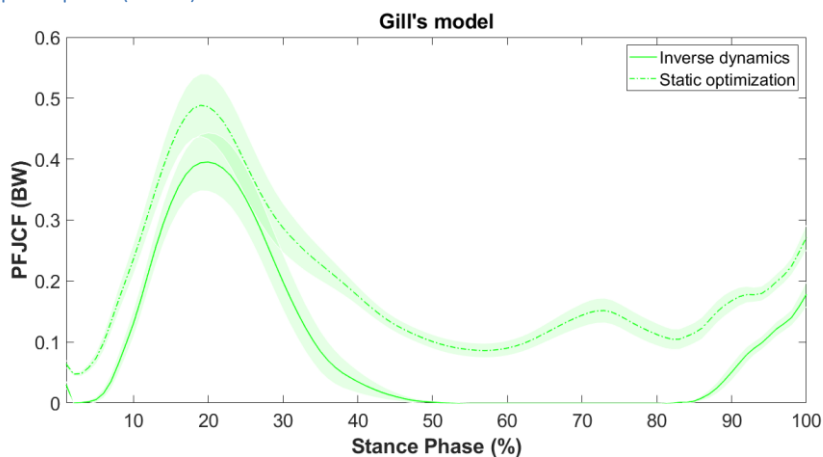
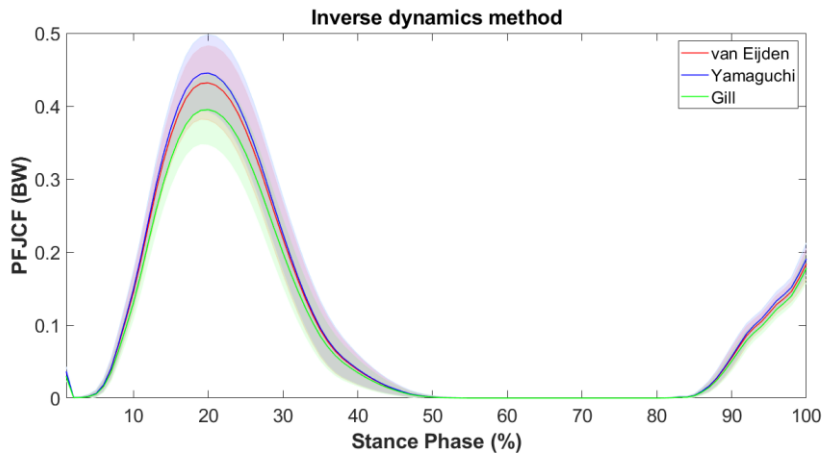
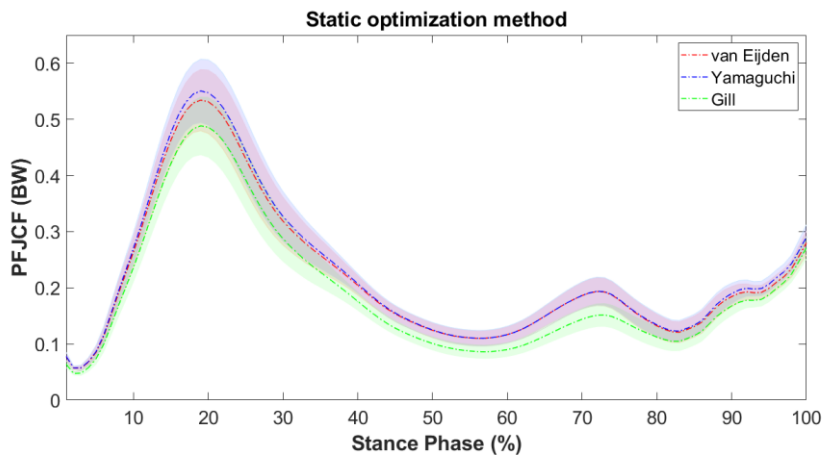


Figure A 8. PFJCF estimated using Gill's model during walking. PFJCF estimated using the inverse dynamics method and static optimization method. The 95% confidence interval of the mean is plotted. The PFJCF is averaged for each trial and for all participants (n=100).



**Figure A 9. PFJCF estimated using the inverse dynamics method during walking.** PFJCF estimated using van Eijden’s, Gill’s and Yamaguchi’s model. The 95% confidence interval of the mean is plotted The PFJCF is averaged for each trial and for all participants (n=100).



**Figure A 10. PFJCF estimated using the static optimization method during walking.** PFJCF estimated using van Eijden’s, Gill’s and Yamaguchi’s model. The 95% confidence interval of the mean is plotted The PFJCF is averaged for each trial and for all participants (n=100).

### Stair Ascending

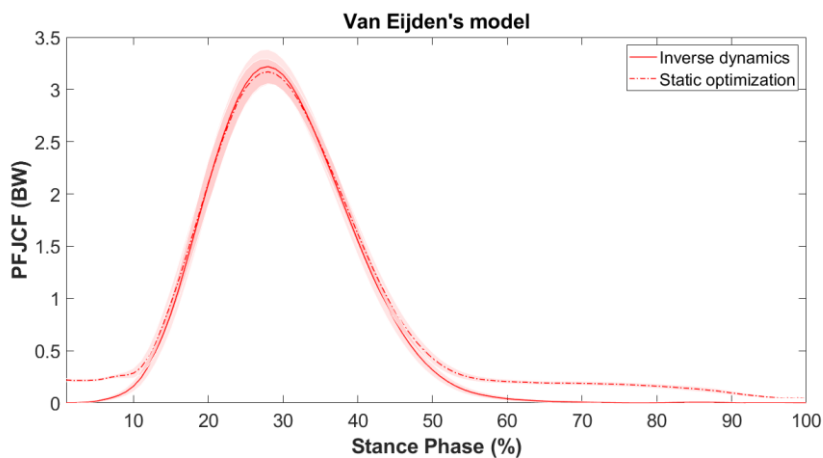


**Figure A 11. PFJCF estimated using van Eijden’s model during stair ascending.** PFJCF estimated using the inverse dynamics method and static optimization method. The 95% confidence interval of the mean is plotted The PFJCF is averaged for each trial and for all participants (n=100).

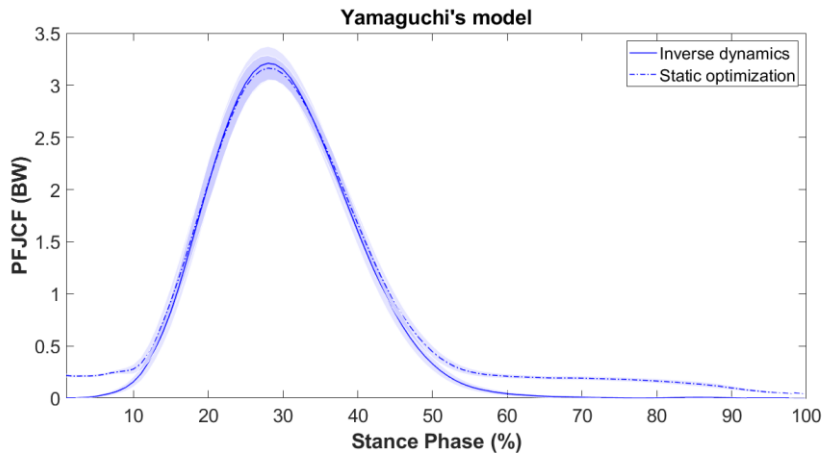


**Figure A 12. PFJCF estimated using Yamaguchi's model during stair ascending.** PFJCF estimated using the inverse dynamics method and static optimization method. The 95% confidence interval of the mean is plotted The PFJCF is averaged for each trial and for all participants (n=100).

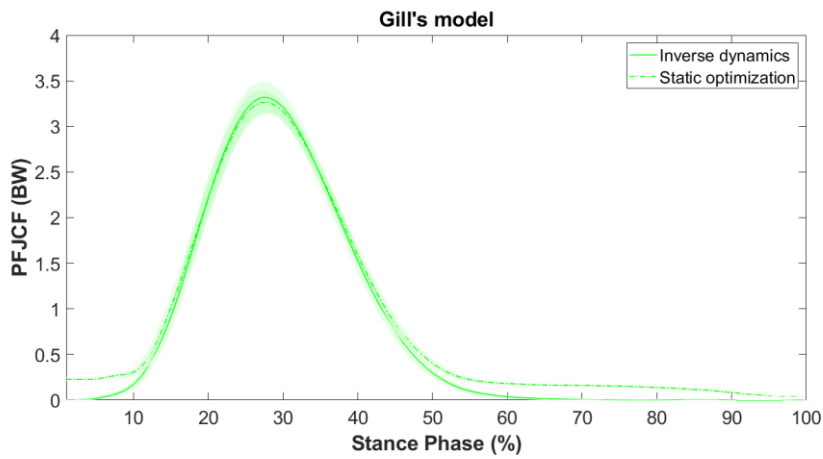


**Figure A 13. PFJCF estimated using Gill's model during stair ascending.** PFJCF estimated using the inverse dynamics method and static optimization method. The 95% confidence interval of the mean is plotted The PFJCF is averaged for each trial and for all participants (n=100).

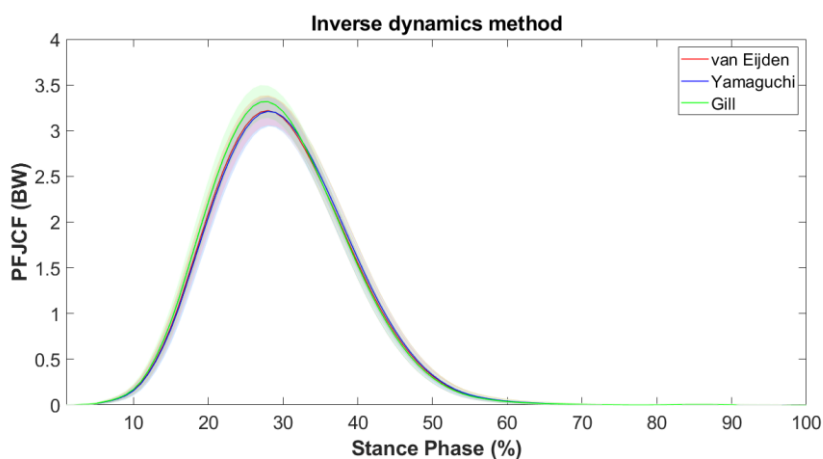


**Figure A 14. PFJCF estimated using the inverse dynamics method during stair ascending.** PFJCF estimated using van Eijden's, Gill's and Yamaguchi's model. The 95% confidence interval of the mean is plotted The PFJCF is averaged for each trial and for all participants (n=100).

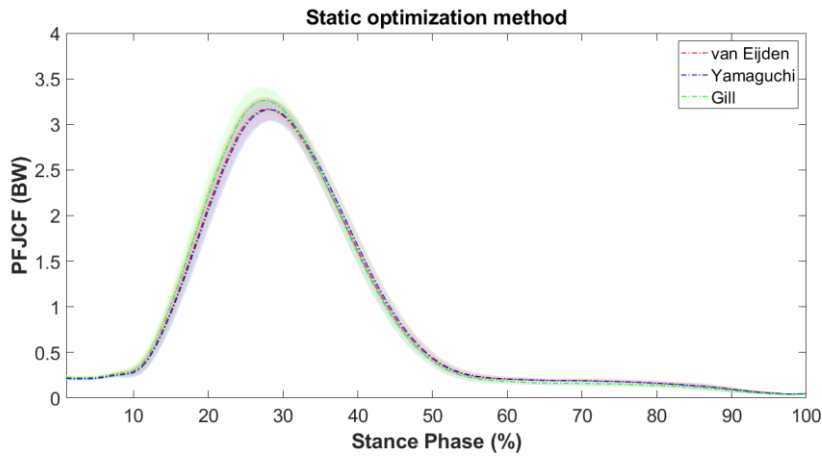


**Figure A 15. PFJCF estimated using the static optimization method during stair ascending.** PFJCF estimated using van Eijden’s, Gill’s and Yamaguchi’s model. The 95% confidence interval of the mean is plotted The PFJCF is averaged for each trial and for all participants (n=100).

### Stair Descending

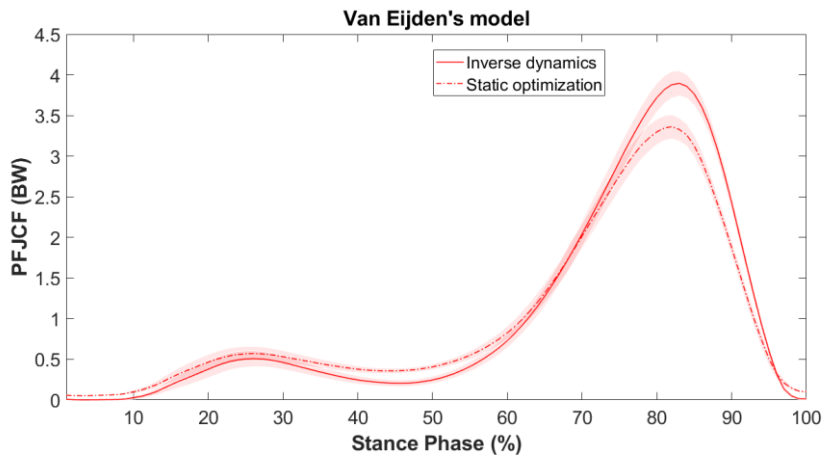


**Figure A 16. PFJCF estimated using van Eijden’s model during stair descending.** PFJCF estimated using the inverse dynamics method and static optimization method. The 95% confidence interval of the mean is plotted The PFJCF is averaged for each trial and for all participants (n=100).

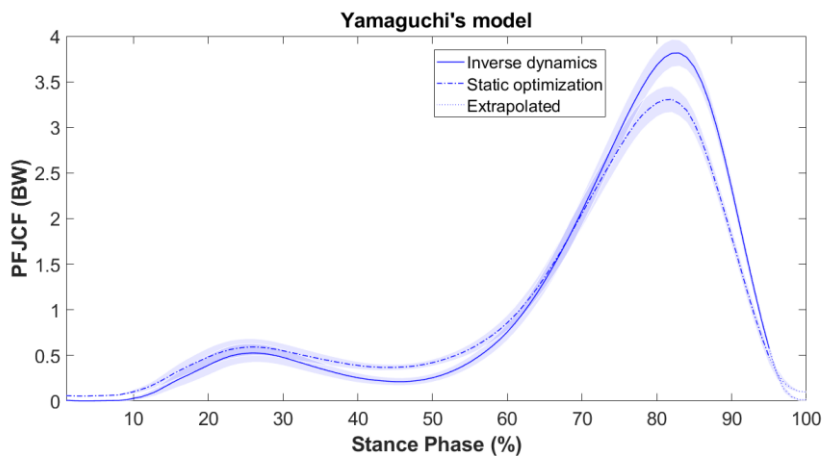


**Figure A 17. PFJCF estimated using Yamaguchi’s model during stair descending.** PFJCF estimated using the inverse dynamics method and static optimization method. The 95% confidence interval of the mean is plotted The PFJCF is averaged for each trial and for all participants (n=100). PFJCF based on Yamaguchi’s model is partly based on the extrapolated P2QFR curve.

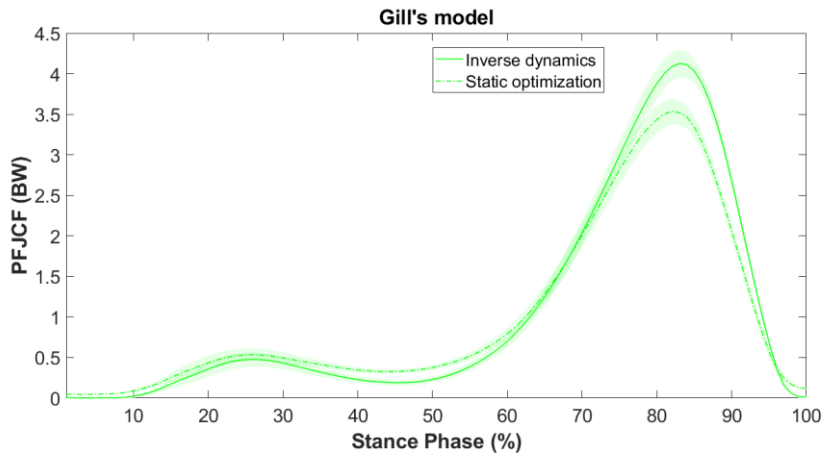


**Figure A 18. PFJCF estimated using van Gill's model during stair descending.** PFJCF estimated using the inverse dynamics method and static optimization method. The 95% confidence interval of the mean is plotted The PFJCF is averaged for each trial and for all participants (n=100).

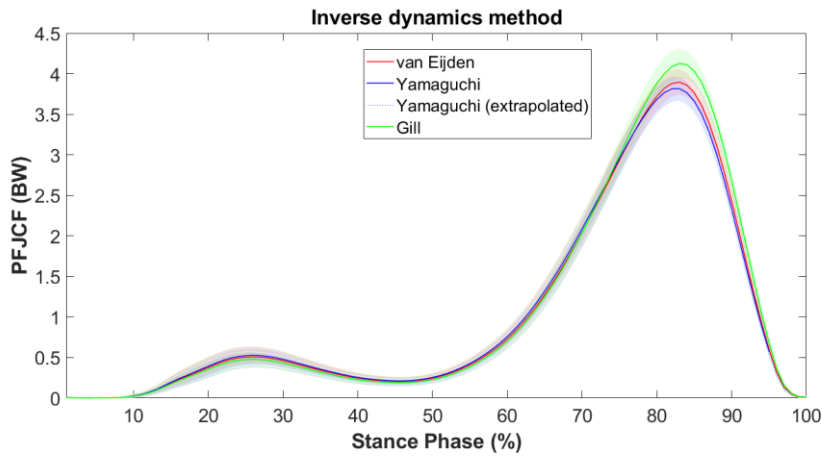


**Figure A 19. PFJCF estimated using the inverse dynamics method during stair descending.** PFJCF estimated using van Eijden's, Gill's and Yamaguchi's model. The 95% confidence interval of the mean is plotted The PFJCF is averaged for each trial and for all participants (n=100). *PFJCF based on Yamaguchi's model is partly based on the extrapolated P2QFR curve.*

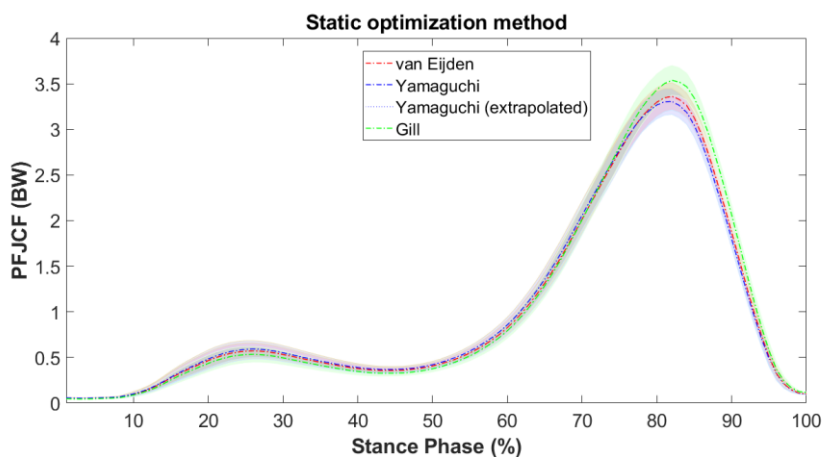


**Figure A 20. PFJCF estimated using the static optimization method during stair descending.** PFJCF estimated using van Eijden's, Gill's and Yamaguchi's model. The 95% confidence interval of the mean is plotted The PFJCF is averaged for each trial and for all participants (n=100). *PFJCF based on Yamaguchi's model is partly based on the extrapolated P2QFR curve.*

## Sit-To-Stand

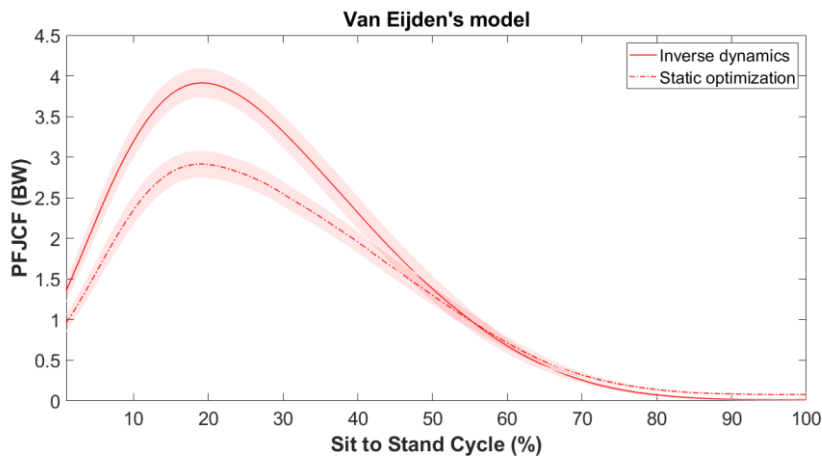


Figure A 21. PFJCF estimated using van Eijden's model during sit-to-stand. PFJCF estimated using the inverse dynamics method and static optimization method. The 95% confidence interval of the mean is plotted. The PFJCF is averaged for each trial and for all participants (n=100).

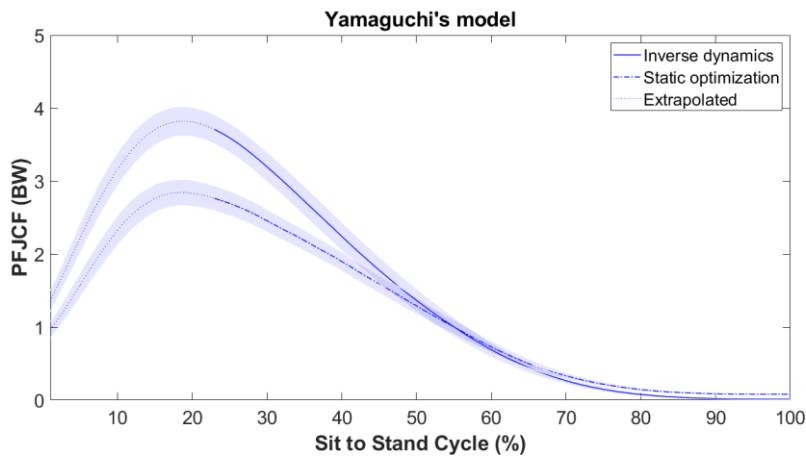


Figure A 22. PFJCF estimated using Yamaguchi's model during sit-to-stand. PFJCF estimated using the inverse dynamics method and static optimization method. The 95% confidence interval of the mean is plotted. The PFJCF is averaged for each trial and for all participants (n=100). PFJCF based on Yamaguchi's model is partly based on the extrapolated P2QFR curve.

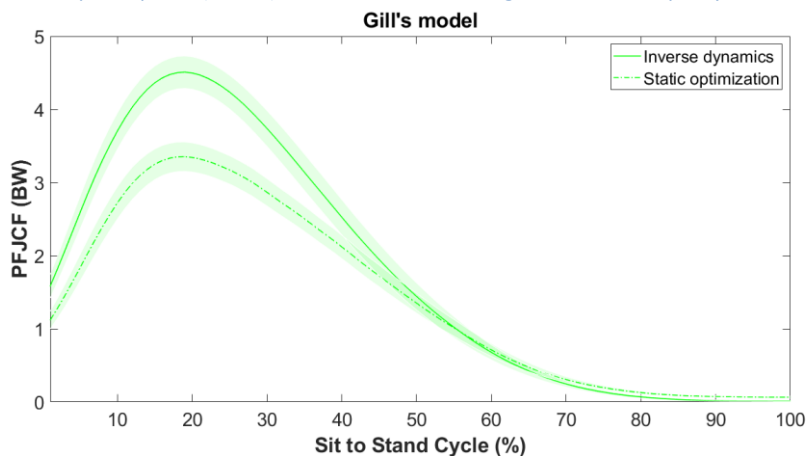
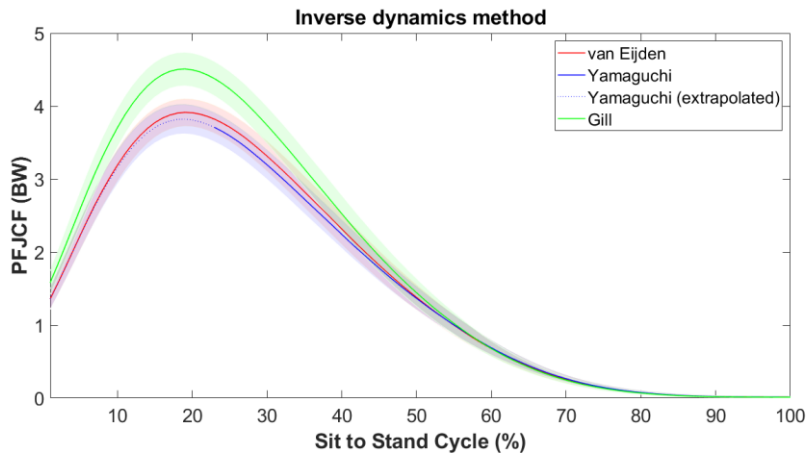
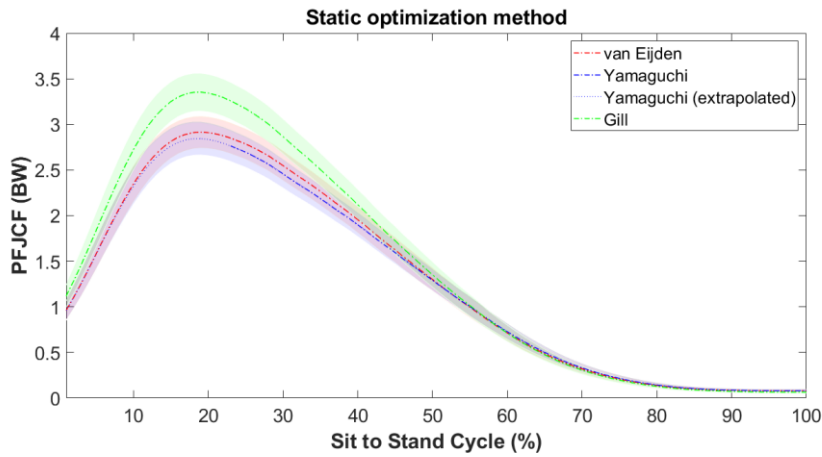


Figure A 23. PFJCF estimated using Gill's model during sit-to-stand. PFJCF estimated using the inverse dynamics method and static optimization method. The 95% confidence interval of the mean is plotted. The PFJCF is averaged for each trial and for all participants (n=100).



**Figure A 24. PFJCF estimated using the inverse dynamics method during sit-to-stand.** PFJCF estimated using van Eijden's, Gill's and Yamaguchi's model. The 95% confidence interval of the mean is plotted The PFJCF is averaged for each trial and for all participants (n=100). *PFJCF based on Yamaguchi's model is partly based on the extrapolated P2QFR curve.*



**Figure A 25. PFJCF estimated using the static optimization method during sit-to-stand.** PFJCF estimated using van Eijden's, Gill's and Yamaguchi's model. The 95% confidence interval of the mean is plotted The PFJCF is averaged for each trial and for all participants (n=100). *PFJCF based on Yamaguchi's model is partly based on the extrapolated P2QFR curve.*

### Stand-To-Sit

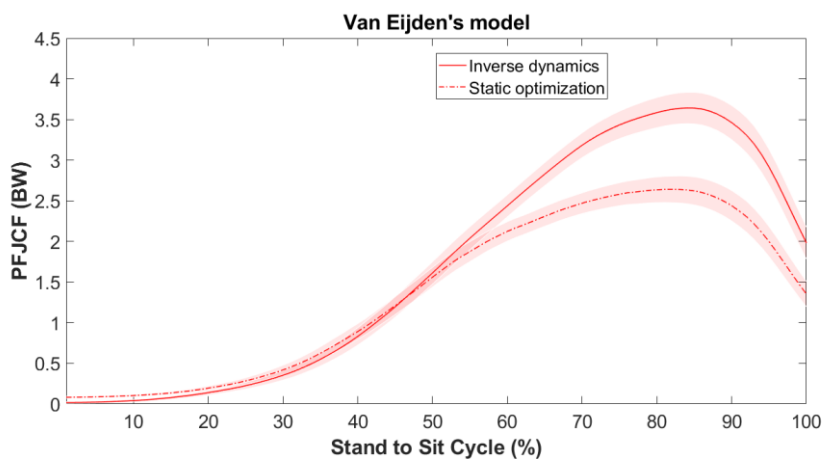


**Figure A 26. PFJCF estimated using van Eijden's model during stand-to-sit.** PFJCF estimated using the inverse dynamics method and static optimization method. The 95% confidence interval of the mean is plotted The PFJCF is averaged for each trial and for all participants (n=100).

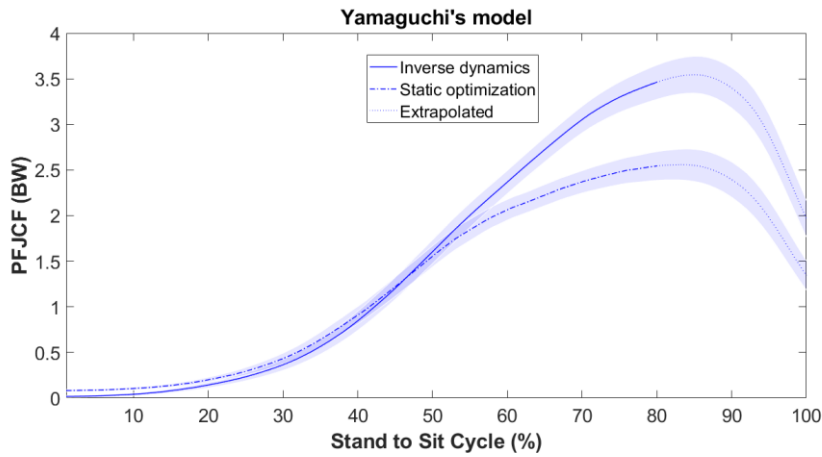


**Figure A 27. PFJCF estimated using Yamaguchi's model during stand-to-sit.** PFJCF estimated using the inverse dynamics method and static optimization method. The 95% confidence interval of the mean is plotted The PFJCF is averaged for each trial and for all participants (n=100). *PFJCF based on Yamaguchi's model is partly based on the extrapolated P2QFR curve.*

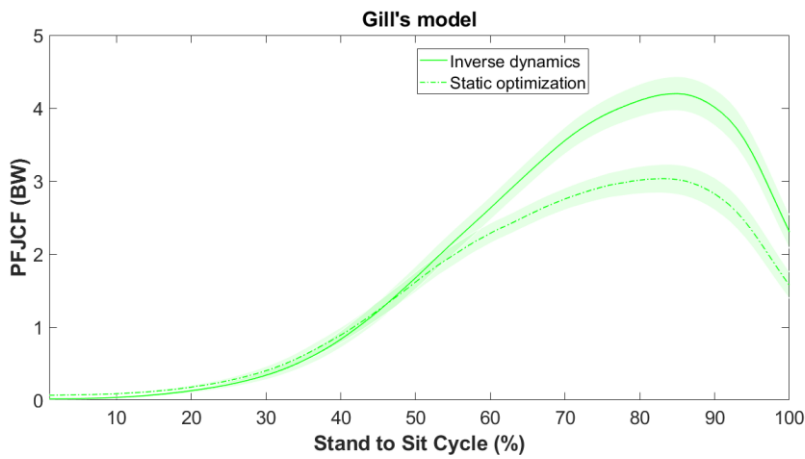


**Figure A 28. PFJCF estimated using Gill's model during stand-to-sit.** PFJCF estimated using the inverse dynamics method and static optimization method. The 95% confidence interval of the mean is plotted The PFJCF is averaged for each trial and for all participants (n=100).

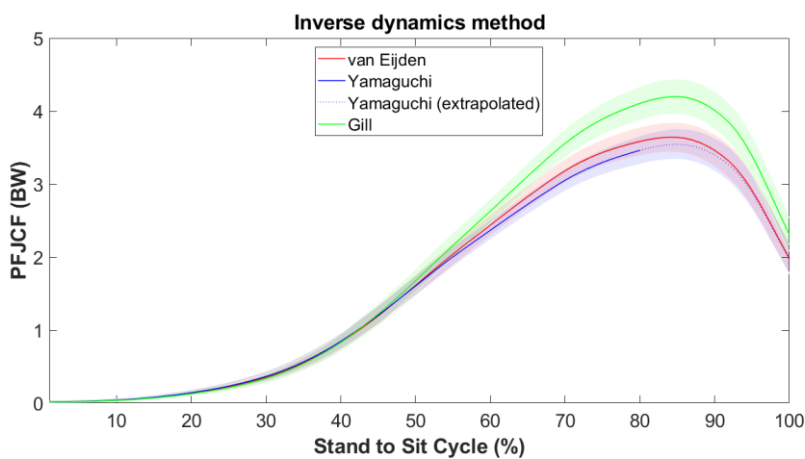


**Figure A 29. PFJCF estimated using the inverse dynamics method during stand-to-sit.** PFJCF estimated using van Eijden's, Gill's and Yamaguchi's model. The 95% confidence interval of the mean is plotted The PFJCF is averaged for each trial and for all participants (n=100). *PFJCF based on Yamaguchi's model is partly based on the extrapolated P2QFR curve.*

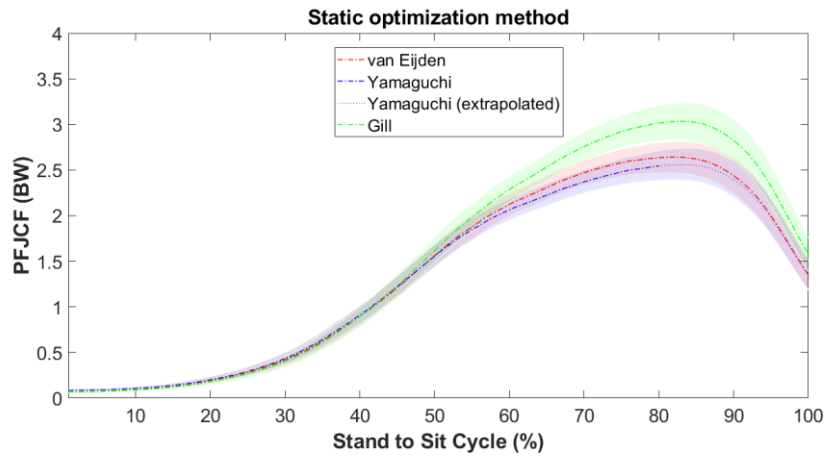


**Figure A 30.** PFJCF estimated using the static optimization method during stand-to-sit. PFJCF estimated using van Eijden's, Gill's and Yamaguchi's model. The 95% confidence interval of the mean is plotted. The PFJCF is averaged for each trial and for all participants (n=100). PFJCF based on Yamaguchi's model is partly based on the extrapolated P2QFR curve.

## Appendix 10 Descriptive results of the peak PFJCF

Table A8. Descriptive results of the peak PFJCF in BW

	Inverse dynamics method				Static optimization method			
	mean	STD	SEM	95% confidence interval	mean	STD	SEM	95% confidence interval
<b>Walking</b>								
van Eijden	0.46	0.25	0.08	[0.30 0.61]	0.56	0.27	0.08	[0.39 0.72]
Yamaguchi	0.47	0.26	0.08	[0.31 0.63]	0.57	0.28	0.09	[0.40 0.75]
Gill	0.42	0.24	0.08	[0.27 0.57]	0.51	0.26	0.08	[0.35 0.67]
<b>Stair Ascending</b>								
van Eijden	3.53	0.63	0.20	[3.14 3.92]	3.45	0.46	0.14	[3.17 3.74]
Yamaguchi	3.51	0.61	0.19	[3.13 3.89]	3.44	0.43	0.17	[3.17 3.71]
Gill	3.66	0.67	0.21	[3.24 4.07]	3.57	0.51	0.16	[3.26 3.89]
<b>Stair descending</b>								
van Eijden	3.99	0.55	0.18	[3.65 4.34]	3.59	0.48	0.15	[3.29 3.89]
Yamaguchi	3.91	0.53	0.17	[3.58 4.24]	3.53	0.47	0.15	[3.24 3.83]
Gill	4.23	0.61	0.19	[3.85 4.61]	3.78	0.51	0.16	[3.46 4.09]
<b>Sit-To-Stand</b>								
van Eijden	4.07	0.79	0.25	[3.59 4.56]	3.07	0.62	0.20	[2.69 3.45]
Yamaguchi*	3.98	0.91	0.29	[3.41 4.54]	3.00	0.72	0.23	[2.56 3.45]
Gill	4.70	0.98	0.31	[4.09 5.30]	3.53	0.75	0.24	[3.07 3.99]
<b>Stand-to-Sit</b>								
van Eijden	3.97	0.75	0.24	[3.50 4.43]	2.90	0.54	0.17	[2.57 3.23]
Yamaguchi*	3.86	0.83	0.26	[3.35 4.38]	2.83	0.61	0.19	[2.46 3.21]
Gill	4.58	0.93	0.29	[4.01 5.15]	3.33	0.66	0.21	[2.92 3.74]

\* Based on the extrapolated curve of Yamaguchi's model.

## Appendix 11 Abbreviations

AIM	Automatic identification of markers
CI	Confidence interval
BW	Body weight
EMG	Electromyographic
MRI	Magnetic resonance imaging
P2QFR	Patellofemoral joint contact force to quadriceps muscle force ratio
PFCA	Patellofemoral contact area
PFJCF	Patellofemoral joint contact force
PFJS	Patellofemoral joint stress
PFOA	Patellofemoral osteoarthritis
PPF	Patellofemoral pain
PT2QFR	Patellar tendon to quadriceps muscle force ratio
QTM	Qualisys Track Manager
ROM	Range of motion
SD	Standard deviation
TFOA	Tibiofemoral osteoarthritis

## Appendix 12 List of Figures, Tables and Equations

### Figures

Figure 1. Osteology of the knee.....	7
Figure 2. The extensor mechanism of the knee.....	8
Figure 3. Patellofemoral joint contact area (PFCA) as a function of the knee flexion angle.....	9
Figure 4. Patellofemoral joint contact force (PFJCF) in the sagittal plane as a function of the knee flexion angle and quadriceps muscle force.....	10
Figure 5. General approach used in studies to estimate the quadriceps muscle force and subsequently the PFJCF (and PFJS).....	11
Figure 6. Experimental set-up.....	17
Figure 7. Marker set of the lower extremity.....	18
Figure 8. The coordinate systems used in QTM and OpenSim.....	19
Figure 9. P2QFR for van Eijden's, Yamaguchi's and Gill's model.....	23
Figure 10. The estimated PFJCF in BW for each activity.....	26
Figure 11. Quadriceps moment arm used in the different estimation methods.....	34
Figure 12. Functions of the P2QFRs of van Eijden's model.....	36
Figure A1. Two-dimensional model of the patellofemoral joint from van Eijden et al. (1986) <sup>[27]</sup> .....	45
Figure A2. Two-dimensional model of the patellofemoral joint from Yamaguchi et al. (1986) <sup>[16]</sup> .....	46
Figure A3. Two-dimensional model of the patellofemoral joint from van Gill et al. (1996) <sup>[26]</sup> .....	47
Figure A4. P2QFR based on Yamaguchi et al. (1989) <sup>[16]</sup> .....	61
Figure A5. P2QFR based on Gill et al. (1996) <sup>[26]</sup> .....	62
Figure A6. PFJCF estimated using van Eijden's model during walking.....	63

Figure A7. PFJCF estimated using Yamaguchi’s model during walking.....	63
Figure A8. PFJCF estimated using Gill’s model during walking.....	63
Figure A9. PFJCF estimated using the inverse dynamics method during walking.....	64
Figure A10. PFJCF estimated using the static optimization method during walking.....	64
Figure A11. PFJCF estimated using van Eijden’s model during stair ascending.....	64
Figure A12. PFJCF estimated using Yamaguchi’s model during stair ascending.....	65
Figure A13. PFJCF estimated using Gill’s model during stair ascending.....	65
Figure A14. PFJCF estimated using the inverse dynamics method during stair ascending....	65
Figure A15. PFJCF estimated using the static optimization method during stair ascending.....	66
Figure A16. PFJCF estimated using van Eijden’s model during stair descending.....	66
Figure A17. PFJCF estimated using Yamaguchi’s model during stair descending.....	66
Figure A18. PFJCF estimated using Gill’s model during stair descending.....	67
Figure A19. PFJCF estimated using the inverse dynamics method during stair descending.....	67
Figure A20. PFJCF estimated using the static optimization method during stair descending.....	67
Figure A21. PFJCF estimated using van Eijden’s model during sit-to-stand.....	68
Figure A22. PFJCF estimated using Yamaguchi’s model during sit-to-stand.....	68
Figure A23. PFJCF estimated using Gill’s model during sit-to-stand.....	68
Figure A24. PFJCF estimated using the inverse dynamics method during sit-to-stand.....	69
Figure A25. PFJCF estimated using the static optimization method during sit-to-stand.....	69
Figure A26. PFJCF estimated using van Eijden’s model during stand-to-sit.....	69

Figure A27. PFJCF estimated using Yamaguchi’s model during stand-to-sit.....	70
Figure A28. PFJCF estimated using Gill’s model during stand-to-sit.....	70
Figure A29. PFJCF estimated using the inverse dynamics method during stand-to-sit.....	70
Figure A30. PFJCF estimated using the static optimization method during stand-to-sit.....	71

## Tables

Table 1. Scaling pairs used in OpenSim.....	20
Table 2. Descriptive results of the peak PFJCF per activity .....	29-30
Table 3. The relative difference in peak PFJCF among the different biomechanical estimation methods .....	30
Table 4. In literature reported peak PFJCF .....	32
Table 5. Knee flexion angle at peak PFJCF.....	35
Table 6. Peak PFJCF in BW for each activity using van Eijden’s model.....	36
Table 7. Summary of the statistical results.....	37
Table T1. Features of the patellofemoral joint models.....	13
Table A1. Participant characteristics.....	48
Table A2. Marker list.....	54
Table A3. List of virtual created markers.....	55
Table A4. List of individual scaling factors.....	56-59
Table A5. Marker weights.....	56
Table A6. Digitized data points of Yamaguchi’s model.....	56
Table A7. Digitized data points of Gill’s model.....	57
Table A8. Descriptive results of the peak PFJCF.....	63

## Equations

Equation 1. Quadriceps muscle force estimation from inverse dynamics.....	11
Equation 2. Effective moment arm calculation.....	12
Equation 3. Least square problem of the inverse kinematics tool of OpenSim.....	21
Equation 4. Equation of motions.....	21
Equation 5. Force velocity and force length constraints used in the static optimization OpenSim.....	22
Equation 6. Cost function used in the static optimization tool of OpenSim.....	22
Equation 7. Effective moment arm of the quadriceps muscle proposed by Brechter and Powers (2002) <sup>[37]</sup> .....	22
Equation 8. PFJCF to quadriceps muscle force ratio based on the patellofemoral joint model of van Eijden et al. (1986).....	23
Equation 9. PFJCF to quadriceps muscle force ratio based on the patellofemoral joint model of Yamaguchi et al. (1989).....	23
Equation 10. PFJCF to quadriceps muscle force ratio based on the patellofemoral joint model of Gill et al. (1996).....	24
Equation 11. Newton's second law.....	35
Equation 12. Newton's second law plus residual forces.....	35